



Contents lists available at ScienceDirect

European Journal of Medicinal Chemistry

journal homepage: <http://www.elsevier.com/locate/ejmech>

Research paper

Novel pyrazolopyridine derivatives as potential angiogenesis inhibitors: Synthesis, biological evaluation and transcriptome-based mechanistic analysis



Maria Michailidou^a, Vassiliki Giannouli^b, Vasilios Kotsikoris^a, Olga Papadodima^c, Georgia Kontogianni^c, Ioannis K. Kostakis^b, Nikolaos Lougiakis^b, Aristotelis Chatziioannou^c, Fragiskos N. Kolisis^d, Panagiotis Marakos^b, Nicole Pouli^{b, **}, Heleni Loutrari^{a, *}

^a GP Livanos and M Simou Laboratories, 1st Department of Critical Care Medicine & Pulmonary Services, Evangelismos Hospital, Faculty of Medicine, National and Kapodistrian University of Athens, 3 Ploutarchou St., 106 75, Athens, Greece

^b Department of Pharmaceutical Chemistry, Faculty of Pharmacy, National and Kapodistrian University of Athens, Panepistimiopolis-Zografou, Athens, 15771, Greece

^c Metabolic Engineering and Bioinformatics Group, Institute of Biology, Medicinal Chemistry and Biotechnology, National Hellenic Research Foundation, 48 Vassileos Constantinou Ave., 116 35, Athens, Greece

^d School of Chemical Engineering, National Technical University of Athens, 9 Iroon Polytechniou, Zografou, 157 80, Athens, Greece

ARTICLE INFO

Article history:

Received 13 April 2016

Received in revised form

15 May 2016

Accepted 18 May 2016

Available online 20 May 2016

Keywords:

Pyrazolo[3,4-c]pyridines

Receptor tyrosine kinase inhibitors

Angiogenesis

Vascular endothelial growth factor

Microarray

Gene ontology

ABSTRACT

Modified purine derivatives exemplified by pyrazolopyrimidines have emerged as highly selective inhibitors of several angiogenic receptor tyrosine kinases. Herein, we designed and synthesized a new series of substituted pyrazolopyridines and explored their ability to influence crucial pro-angiogenic attributes of endothelial cells. Four of the synthesized compounds, possessing analogous substitution pattern, were found able to inhibit at low micromolar concentrations endothelial cell proliferation, migration and differentiation, constitutively or in response to Vascular Endothelial Growth Factor (VEGF) and to attenuate VEGF-induced phosphorylation of VEGF receptor-2 and downstream kinases AKT and ERK1/2. Administration of effective compounds in mice delayed the growth of syngeneic Lewis lung carcinoma transplants and reduced tumor microvessel density, without causing toxicity. Genome-wide microarray and gene ontology analyses of treated endothelial cells revealed derivative **18c** as the most efficient modulator of gene expression and “mitotic cell cycle/cell division” along with “cholesterol biosynthesis” as the most significantly altered biological processes.

© 2016 Elsevier Masson SAS. All rights reserved.

Abbreviations: VEGF, Vascular Endothelial Growth Factor; VEGFR, Vascular Endothelial Growth Factor receptor(s); EC, endothelial cells; RTK, receptor Tyr kinase; FDA, United States Food and Drug Administration; HUVEC, human umbilical vein endothelial cells; MTT, 3-(4,5-dimethylthiazol-2-yl)-2,5-diphenyltetrazolium bromide; LLC, Lewis lung carcinoma; GO, gene ontology; qRT-PCR, real-time quantitative reverse PCR; HMGCS, hydroxy-3-methylglutaryl-CoA synthase 1; MSMO1, methylsterol monooxygenase; INSIG1, insulin induced gene 1; SQLE, squalene epoxidase; UBE2C, ubiquitin-conjugating enzyme E2C; CCNB2, cyclin B2; CCNA2, cyclin A2; CDC20, cell division cycle 20; HMOX1, heme oxygenase 1; Pddb, bis(dibenzylideneacetone)palladium; X-Phos, 2-dicyclohexylphosphino-2',4',6'-triisopropylbiphenyl; Et₂O, diethyl ether; NIS, N-iodosuccinimide.

* Corresponding author.

** Corresponding author.

E-mail addresses: mmichail@med.uoa.gr (M. Michailidou), v_giannouli@yahoo.gr (V. Giannouli), vasiliskotsikoris@yahoo.gr (V. Kotsikoris), opapadod@eie.gr (O. Papadodima), gkontogianni@eie.gr (G. Kontogianni), ikkostakis@pharm.uoa.gr (I.K. Kostakis), nlougiak@pharm.uoa.gr (N. Lougiakis), achatzi@eie.gr (A. Chatziioannou), kolisis@chemeng.ntua.gr (F.N. Kolisis), marakos@pharm.uoa.gr (P. Marakos), pouli@pharm.uoa.gr (N. Pouli), elloutrar@med.uoa.gr (H. Loutrari).

<http://dx.doi.org/10.1016/j.ejmech.2016.05.035>

0223-5234/© 2016 Elsevier Masson SAS. All rights reserved.

1. Introduction

Angiogenesis, the formation of new blood vessels from pre-existing vasculature, has become an important therapeutic target because of its crucial role in several pathologies, characteristically in tumor progression and metastasis [1]. As a result the discovery of new compounds possessing potent anti-angiogenic activity has been the focus of intense current research [2–6]. Numerous growth factors are involved in tumor angiogenesis such as Vascular Endothelial Growth Factor (VEGF) [7], epidermal growth factor [8], platelet-derived growth factor [9], and basic fibroblast growth factor [10]. Yet, the members of VEGF family including VEGF-A, B, C, D, E and placenta growth factor are considered to be the most critical endothelium-specific mediators of angiogenesis [7]. VEGF exerts its biological effects by binding to and activating VEGF receptors (VEGFR) which are almost exclusively expressed in endothelial cells (EC). There are three types of VEGFR, namely, VEGFR1 (Flt-1), VEGFR2 (KDR/Flk-1) and VEGFR3. Among them, VEGFR2 plays a major role in VEGF-A-mediated vascular cell biology [11,12]. Binding of VEGF-A to VEGFR2 results in the activation of several signal transduction events. These involve receptor dimerization and autophosphorylation at specific Tyr residues followed by phosphorylation of downstream proteins including PKC, phospholipase C γ , PI3K, 3-phosphoinositide-dependent kinase 1, AKT, focal adhesion kinase, ERK1/2, Src and p38MAPK [13–16]. More specifically, activation of PI3K–AKT cascade by VEGFR2 has been shown to play a causal role in VEGF-stimulated survival, migration and sprouting of endothelial cells in vitro and angiogenesis in vivo, whereas VEGF-induced ERK1/2 and p38MAPK signaling have been mostly associated with regulation of EC proliferation and motility, respectively [11,12]. Consequently, VEGF and VEGFR2 signaling system is recognized as an attractive target for anti-angiogenic intervention and a variety of approaches are currently being assessed in cancer clinical trials. These include the use of soluble VEGFR, monoclonal antibodies against VEGF or VEGFR and small molecule inhibitors of VEGFR Tyr kinase activity [17–19].

In recent years targeted inhibition of several oncogenic receptor Tyr kinases (RTK) by small molecules that compete with the ATP for binding in the catalytic domain has been introduced as a systemic treatment strategy for cancer. Actually, an array of RTK inhibitors are being studied in clinical trials whereas several of them such as sorafenib and sunitinib (Chart 1) have already been approved by the United States Food and Drug Administration (FDA) for indication of specific types of cancer [20]. Nevertheless limitations in the use of these targeted therapies, mostly associated with clinical resistance and toxicity [21], prompt the need for developing new drug candidates with improved bioactivity and a more favorable safety profile. Pyrazolo[3,4-*d*]pyrimidines through their selectivity toward different RTK have proved to be a very promising chemical class in the discovery of new lead compounds to treat cancer and pathological angiogenesis [22,23].

Focusing on VEGFR inhibitors, a great number of ATP site-targeted ligands have been produced using either analogue synthesis approaches or a combination of more sophisticated methods, including structure-based drug design and fragment-based strategies. Among them, some disubstituted 6-aminopurines [24] and trisubstituted pyrazolo[4,3-*d*]pyrimidines [25] inhibit tumor angiogenesis and cell migration, whereas benzothioopyrano[4,3-*d*]pyrimidines [5] and 3-aminopyrazolo[3,4-*b*]pyridine ureas [26] target kinases of the VEGF pathway. Closely related to the later, pyrrolo[3,2-*d*]pyrimidine derivatives display strong inhibitory activities against both VEGFR and fibroblast growth factor receptor kinases [27] and possess anti-proliferative activity against VEGF-stimulated human umbilical vein endothelial cells (HUVEC) [28]. In this respect the study of bioisosters provides an important tool

for the complete investigation of the bioactivity and the discovery of new/modified derivatives with improved properties.

As part of our involvement in the design and synthesis of new potentially bioactive purine analogues [29–31], we report here the synthesis and evaluation of a number of novel pyrazolo[3,4-*c*]pyridine derivatives as angiogenesis inhibitors. To this end we initially examined the ability of this class of compounds to affect essential pro-angiogenic functions of EC, constitutively or upon stimulation with VEGF in cell-based assays and next to modulate tumor angiogenesis and growth in a mouse cancer model. Finally, we analyzed the global effect of best candidates on EC transcriptome in an effort to uncover potential action mechanisms. Our study may provide a basis for further evaluation of the most promising derivative(s) in anti-angiogenic therapeutic interventions, especially for cancer treatment.

2. Results and discussion

2.1. Chemistry

The target compounds were prepared using 2-amino-5-nitro-4-picoline (**1**, Scheme 1) [32] as starting material. This compound was diazotized and the resulting pyridinone **2** [33] was treated with phosphorus oxychloride and converted to the chloropicoline **3** [34].

The nitroderivative **3** was then reduced using stannous chloride as the reducing agent to give the aminopyridine **4** which was acetylated to the acetamide **5**. This acetamide was then heated at reflux in benzene with isoamyl nitrite, in the presence of acetic anhydride [35,36]. This furnished a mixture of the corresponding 1- and 2-acetylpyrazolo[3,4-*c*]pyridines through a rearrangement of the intermediate *N*-nitroso compound. These isomers were not isolated, but the acetyl groups were easily cleaved upon treatment with methanolic ammonia to provide the pyrazolopyridine **6** [36]. Compound **6** was subsequently treated with 4-methoxybenzyl chloride in the presence of sodium hydride to provide derivative **7**, together with an amount of the corresponding *N*2 regio-isomer. From a brief study of the reaction conditions we resulted that the use of a polar solvent (DMF) at room temperature favors the formation of *N*1 over *N*2 isomer, which was thus prepared in 2:1 ratio. Both isomers were separated and identified using NOE spectroscopic data. More precisely, in the case of the *N*1-isomer we recorded a clear cross-coupling of both the benzylic and *o*-phenyl protons with H-7. Compound **7** was then converted to the corresponding *N*-oxide **8**, using *m*-CPBA as oxidizing agent. The rearrangement of the *N*-oxide in the presence of phosphorous oxychloride, produced the 5,7-dichloropyrazolopyridine **9**, which was used for the nucleophilic substitution of the 7-chloro group using suitable secondary amines, in order to provide compounds **10a–c**. The chlorides **10** were converted to the target derivatives **11a–d** through a Suzuki-type coupling with aniline or 4-(4-methylpiperazin-1-yl)aniline, in the presence of cesium carbonate, using bis(dibenzylideneacetone)palladium (Pddba) [37] as catalyst and 2-dicyclohexylphosphino-2',4',6'-triisopropylbiphenyl (X-Phos) as ligand [38]. ¹H and ¹³C NMR spectra of target compounds **11a–d** are provided in Supplementary data.

The corresponding 3-phenyl analogues (**18a–c**, Scheme 2), were prepared from the intermediate chloride **6**, which was successively converted to the iodide **12** upon treatment with *N*-iodosuccinimide and then to the 4-methoxybenzyl derivative **13** [39]. This iodide provided the 3-phenylanalogue **14**, through a Suzuki-type coupling using phenylboronic acid in the presence of tetrakis(-triphenylphosphine)palladium (0) and sodium bicarbonate. Following a synthetic procedure analogous to the above mentioned one, analogue **14** was converted to the target derivatives **18a–c**. ¹H and ¹³C NMR spectra of target compounds **18a–c** are provided in

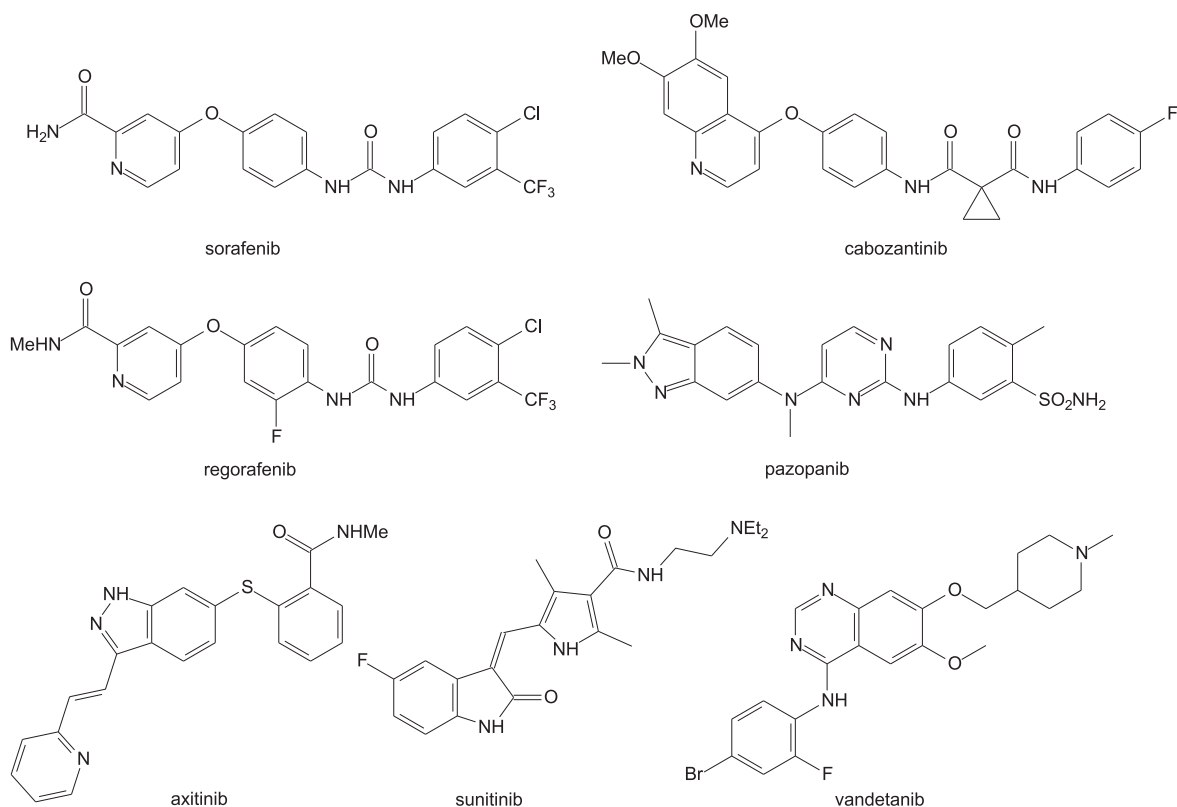
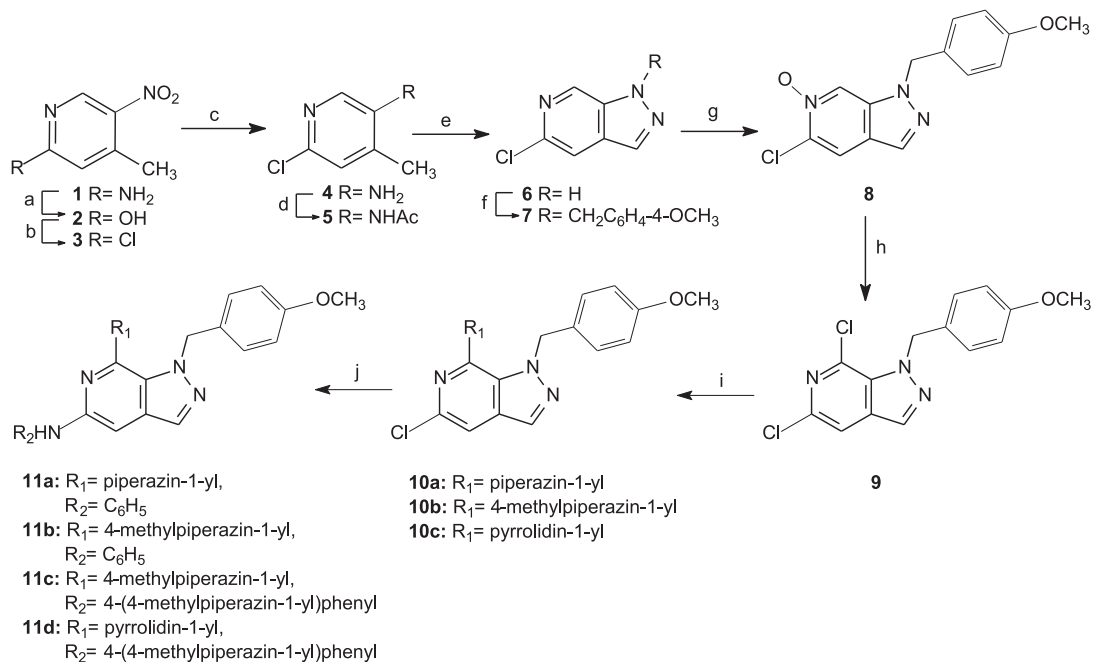
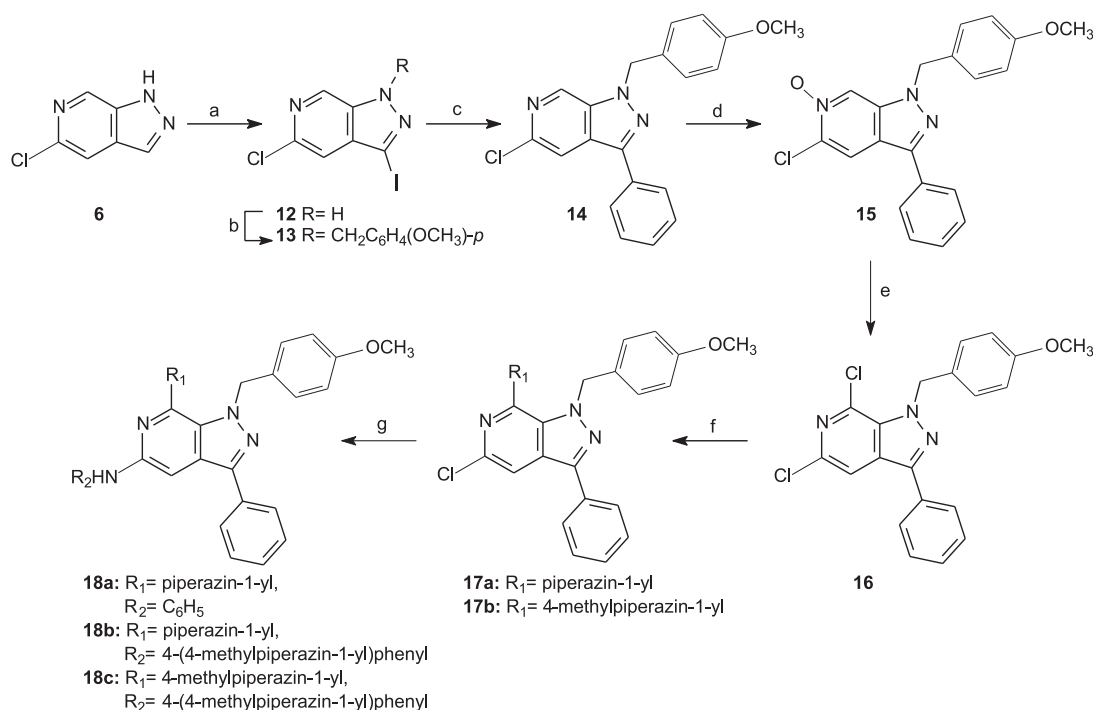


Chart 1. Representative structures of FDA approved anti-angiogenic drugs.



Scheme 1. Reagents and conditions: a) NaNO₂, H₂SO₄, H₂O; b) POCl₃, 110 °C; c) SnCl₂·2H₂O, HCl(c), 55 °C; d) Ac₂O, CH₂Cl₂, r.t.; e) i) AcOK, Ac₂O, isoamyl nitrite, benzene, reflux, ii) NH₃(g.), MeOH, r.t.; f) i) NaH, DMF, r.t., ii) 4-methoxybenzyl chloride, DMF, r.t.; g) *m*-CPBA, CHCl₃, r.t.; h) POCl₃, THF, r.t.; i) piperazine (for **10a**) or pyrrolidine (for **10c**), microwave irradiation, 300 W, 160 °C, or *N*-methylpiperazine (for **10b**), reflux; j) aniline (for **11a**, **11b**) or 4-(4-methylpiperazin-1-yl)aniline (for **11c**, **11d**), X-Phos, Pd(dba)₃, CsCO₃, toluene, reflux.



Scheme 2. Reagents and conditions: a) NIS, MeOH, r.t.; b) i) NaH, DMF, r.t., ii) 4-methoxybenzyl chloride, DMF, r.t.; c) phenylboronic acid, Pd(PPh₃)₄, NaHCO₃, toluene/ethanol/H₂O (10/1/0.2), reflux; d) *m*-CPBA, CHCl₃, r.t.; e) POCl₃, THF, r.t.; f) piperazine (for **17a**) or *N*-methylpiperazine (for **17b**), microwave irradiation, 300 W, 160 °C; g) aniline (for **18a**) or 4-(4-methylpiperazin-1-yl)aniline (for **18b**, **18c**), X-Phos, Pd(dba)₃, CsCO₃, toluene, reflux.

Supplementary data.

2.2. Biological evaluation

2.2.1. Cellular assays and angiogenesis models

The newly synthesized pyrazolopyridines **10a**, **11a-d**, **17a** and **18a-c** were initially screened for their ability to modulate the proliferative and migratory competence of EC, at two representative concentrations (0.2 and 2 μM), under non-induced conditions i.e. in response to culture medium supplemented with a low content of fetal bovine serum (2.5–5%). As shown in Fig. 1 from the nine compounds tested, only the 3-phenylsubstituted derivatives **17a** and **18a-c** were found able to significantly inhibit both the EC growth (A) and migration (B) in the applied *in vitro* assays, indicating that 3-phenyl group substitution is required for anti-angiogenic activity. Thus, these four derivatives were subsequently chosen for a more detailed evaluation of their anti-angiogenic actions and underlying mechanisms. IC₅₀ values for cytostatic activity of the best inhibitors determined under similar non-induced conditions were found to be in the low micromolar range (Table 1).

Next, in order to explore whether the four selected anti-angiogenic pyrazolopyridines could specifically attenuate the VEGF-A-driven activation of pro-angiogenic endothelial phenotypes, we examined the capability of compound-treated EC to proliferate, migrate, and develop tube-like networks in response to exogenously added VEGF-165, the most abundant variant of VEGF-A. Cell growth studies conducted by the MTT method (Fig. 2A) demonstrated that derivatives **17a**, **18a** and **18c** were able to significantly impair the stimulatory effect of VEGF-165 on HUVEC growth, thus indicating an inhibitory action in cell proliferation and/or survival. However compound **18c** proved to be the most effective inhibitor in the examined range of concentrations (0.5–2.0 μM). Similar results were obtained using CyQUANT® cell

proliferation assay that is based on DNA content (not shown). Furthermore, all four compounds were found to drastically decrease VEGF-165-induced HUVEC chemotactic migration in Transwell assays (Fig. 2B) and abolish the stimulatory action of VEGF-165 on HUVEC characteristic ability to differentiate into capillary-like structures when cultured on a Matrigel-coated surface (Fig. 2C).

Because VEGFR2 is the main mediator of VEGF-A-triggered endothelial growth, motility and functional differentiation [11,12] these results pointed to the hypothesis that in VEGF-A-induced HUVEC test pyrazolopyridines exert their inhibitory actions mainly by targeting RTK activity of VEGFR2 in HUVEC. However interference of these derivatives with other endothelial RTK cannot be certainly excluded. As a matter of fact in preliminary *in vitro* data using a commercially available assay kit we found that the selected compounds were able to significantly suppress the total protein Tyr kinase activity in treated HUVEC, though they displayed a quite different effect within the examined range of concentrations (Supplementary data, Fig. S1). In order to directly evaluate our hypothesis about VEGFR2 targeting, we subsequently assessed the effect of active compounds on the extent of VEGFR2 autophosphorylation at key Tyr residues (Tyr951, Tyr996, Tyr1059 and Tyr1175) after stimulation of HUVEC with VEGF-165. As shown in Fig. 3A all test compounds significantly inhibited the relative phosphorylation levels of Tyr1175, known to be essential for the activation of VEGFR2 signal transduction and subsequent control of endothelial functions [13,15], without affecting the amount of total VEGFR2 in cell lysates. No significant changes were observed in the relative phosphorylation levels of Tyr951, Tyr996 (with the exception of **18b**) and Tyr1059. To further investigate the consequences of the observed inhibitory effect on VEGFR2 signal transduction, we next examined whether these compounds could modulate the relative phosphorylation of three key downstream substrates, namely ERK1/2, AKT and p38MAPK. As shown in Fig. 3B compound

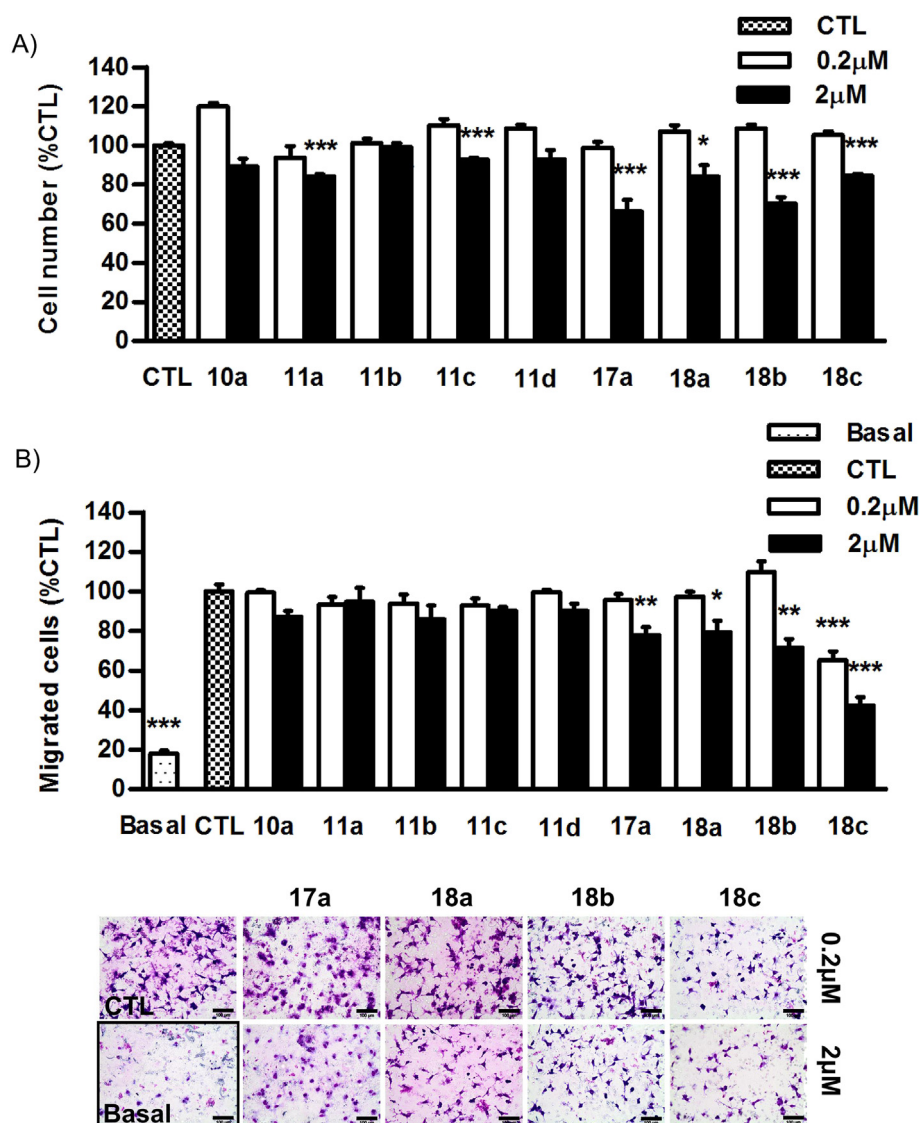


Fig. 1. Screening for angiogenesis modulators. (A) Effects of compounds on EC proliferation. EA.hy926 cells were treated with compound or DMSO (CTL) in medium containing 2.5% FBS for 48 h. Data represent mean % of cell number relative to CTL \pm SEM of replicates from two independent experiments (* $p < 0.05$, ** $p < 0.01$, *** $p < 0.001$). (B) Effects of compounds on EC migration. HUVEC pre-treated with compound or DMSO (CTL) were allowed to migrate towards medium containing 5% FBS or starvation medium (Basal). Graphs represent mean % of migrating cells relative to CTL \pm SEM from replicates of two independent experiments (* $p < 0.05$, ** $p < 0.01$, *** $p < 0.001$). In the lower panel, representative microphotographs of migrating cells (magnification $\times 200$; scale bar: 100 μ m).

Table 1
IC₅₀ values (μ M) for anti-proliferating activity^a of compounds **17a** and **18a-c**.

17a	18a	18b	18c
4.3 \pm 0.3	14.1 \pm 0.9	12.0 \pm 0.6	7.2 \pm 2.4

^a EC were treated with test compounds at a range of concentrations (0.125–50 μ M). Cell proliferation was assessed by the 3-(4,5-dimethylthiazol-2-yl)-2,5-diphenyltetrazolium bromide (MTT) method. Values represent mean \pm SEM.

treatment resulted in a marked inhibition of VEGF-165-induced phosphorylation of AKT and ERK1/2, known to promote endothelial cell survival, migration and proliferation [11], but did not affect the phosphorylation of p38MAPK. Overall, these data provide direct evidence that in VEGF-simulated EC test compounds efficiently impede RTK activity of VEGFR2 consequently leading to disturbance of activation of ERK1/2 and AKT signaling and subsequent inhibition of related angiogenic functions.

Finally, we examined the anti-tumor and anti-angiogenic

potential of the four selected inhibitors in vivo, using a well-characterized late-stage preclinical model based on Lewis lung carcinoma (LLC) cell transplantation into immunocompetent mice. Administration of test compounds into tumor-bearing C57BL/6 mice significantly reduced the rate of tumor growth, with the exception of derivative **18a** that was less effective (Fig. 4A). None of the compounds created signs of toxicity as assessed by the clinical examination and haematoxylin-eosin staining of tissue sections from vital organs (not shown). Furthermore, IHC analysis of tumor sections using CD31-specific antibody staining showed a concomitant significant decrease of microvessel density in tissues from mice treated with active compounds as compared to tumors from vehicle-treated animals (Fig. 4B). Collectively, derivatives **17a**, **18b** and **18c** proved to be capable of delaying LLC tumor growth in mice, to some extent, through a remarkable inhibition of tumor vascularization, in good correlation with our preceding in vitro data and were selected for further investigation.

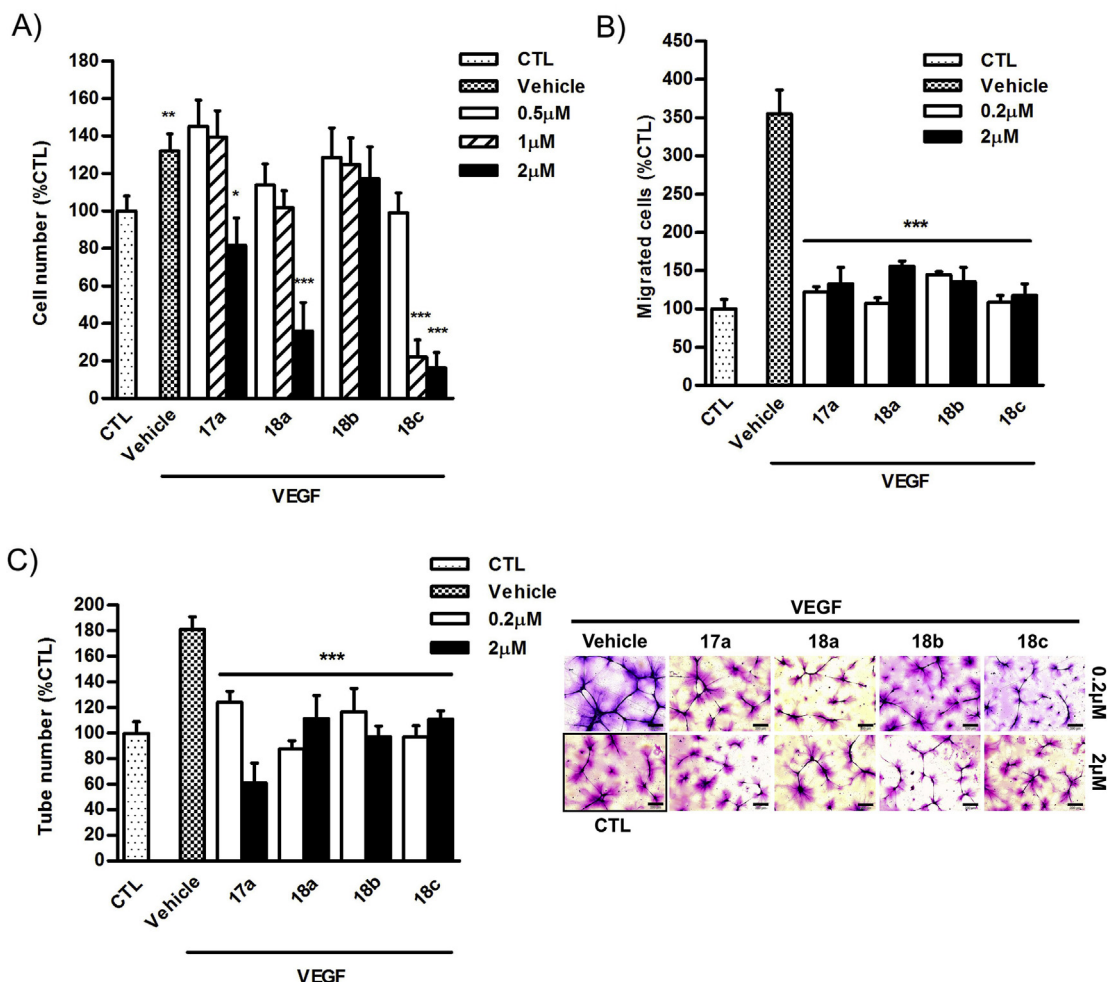


Fig. 2. Effects of best inhibitors on VEGF-induced EC functions. (A) EC proliferation. HUVEC were treated with compound or DMSO vehicle in starvation medium containing or not VEGF-165 for 48 h. Data represent mean % of cell number relative to control (vehicle in starvation medium, CTL) \pm SEM of replicates from at least two independent experiments (* $p < 0.05$, ** $p < 0.01$; *** $p < 0.001$ in relation to vehicle-VEGF-165). (B) EC migration. HUVEC pre-treated with compound or DMSO were allowed to migrate towards medium supplemented with VEGF-165 or starvation medium (CTL). Data represent the mean % of migrated cells relative to CTL \pm SEM of replicates from at least two independent experiments (*** $p < 0.001$ in relation to vehicle-VEGF-165). (C) EC differentiation. HUVEC cultured on Matrigel-coated surfaces were treated with compound or DMSO in the presence or not of VEGF-165 for 24 h. Graphs represent mean % of tube number relative to control (vehicle in medium, CTL) \pm SEM of replicates from two independent experiments (* $p < 0.05$; ** $p < 0.01$; *** $p < 0.001$ in relation to vehicle-VEGF-165). On the right panel, representative microphotographs of tube-like networks (magnification $\times 100$; scale bar: 200 μ m).

2.2.2. Genome-wide microarray and gene ontology (GO) analyses

In an effort to explore the mechanisms underlying the phenotypic changes imposed by the best three candidates, we next examined by genome-wide microarrays the differential gene expression profile of treated EC at two different time points, 6 h and 24 h.

As demonstrated in Table 2, derivative **18c** had the most pronounced effect on gene expression affecting a total number of 256 genes (12 were common in both time points), followed by **17a** and **18b** (33 and 17 altered genes, respectively). Complete lists of significantly modified genes, are provided in Supplementary data (Tables S1, S2 and S3) while the entire microarray dataset has been deposited in NCBI's Gene Expression Omnibus (GEO) and is accessible through GEO accession number GSE75588.

We next analyzed the union of differentiated probes, meaning those that were significant at least once, by hierarchical clustering. As shown in the heat map representation of gene expression fold-change values (Fig. 5), there is a significant cluster of under-expressed genes common in all three compounds following 24 h of exposure. Moreover, pathway analysis, exploiting the functional annotations of GO, revealed that this cluster of altered genes affects

cellular functions pertinent to mitosis and cell division ("mitotic cell cycle", "cell division", "mitotic nuclear division", etc), suggesting a down-regulating effect on cell proliferation, in concurrence with our preceding experimental results (Figs. 1A and 2A).

We then focused on the dataset from cells treated with **18c** for 24 h, because it enclosed the highest number of differentially expressed genes and performed a detailed functional analysis in order to gain insight into the affected molecular processes. Fig. 6 depicts bar plots of the top enriched processes with the amount of differentially expressed genes per GO term. The biological processes that were mostly deregulated by **18c** fall into two basic categories: a. those that, consistent with our experimental data, were related to mitosis and included in vast majority under-expressed genes, such as "mitotic cell cycle" involving 39 genes (Supplementary data, Table S4) and b. those generally related to cholesterol and lipid metabolism which contained almost exclusively over-expressed genes, such as "cholesterol biosynthetic process" involving 17 genes (Supplementary data, Table S5). Although additional mechanistic studies are certainly required, this finding corroborates the acquired phenotypic data since cholesterol homeostasis and in general endothelial cell metabolism have been

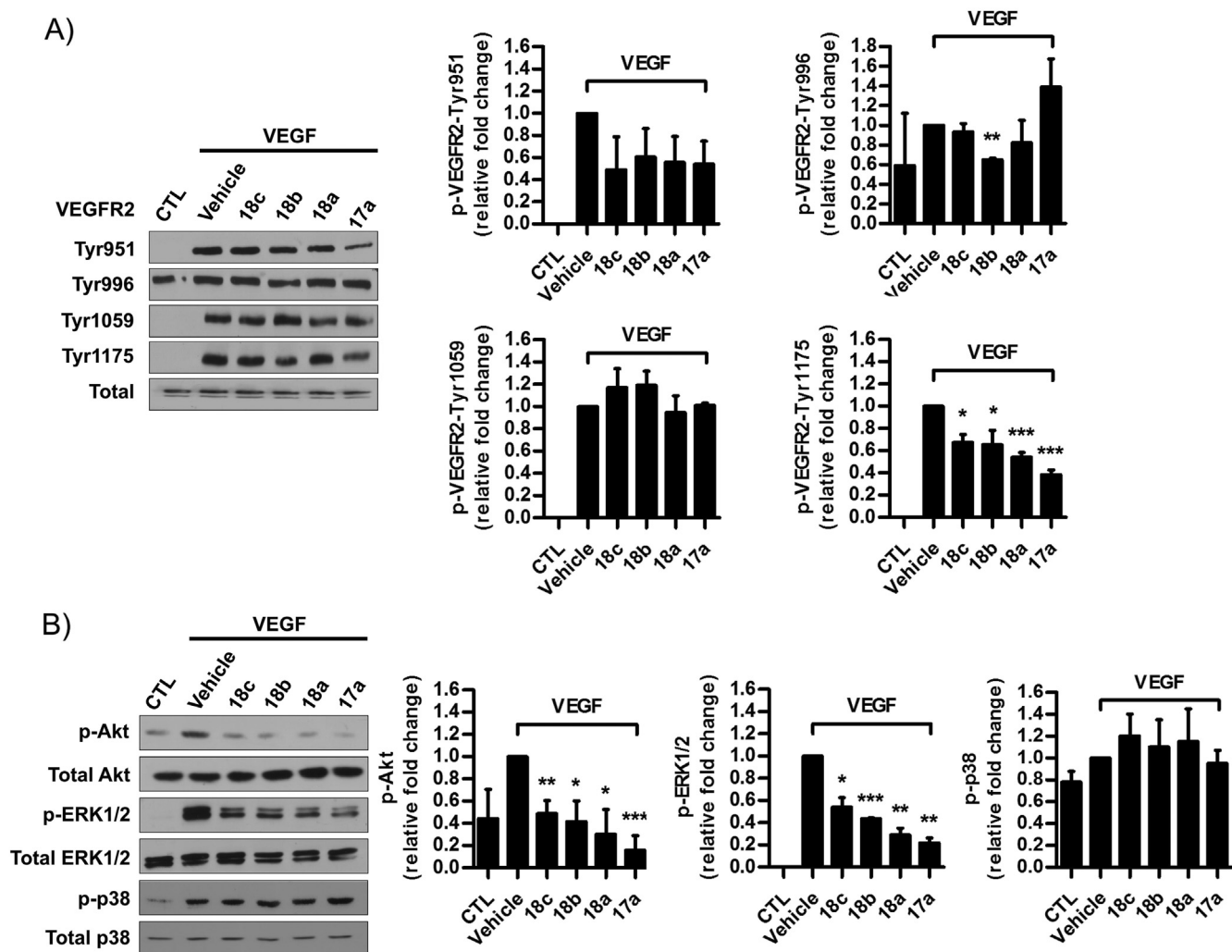


Fig. 3. Effects of **17a** and **18a-c** on VEGF-induced phospho-signaling. Western blot analysis of protein extracts from HUVEC pre-treated with 2 μ M of test compound or DMSO vehicle for 2 h and then exposed to VEGF-165 or vehicle containing medium (CTL) for 5 min. (A) Detection of phosphorylated VEGFR2 at indicated Tyr residues. (B) Detection of phosphorylated AKT, ERK1/2 and p38MAPK. Blots shown are representative of at least three independent experiments. Graphs are mean data from densitometry analysis and demonstrate relatively changed phosphorylation levels of shown protein by test compound when the level of VEGF-induced protein phosphorylation in the absence of compound, was normalized as 1.0. All phosphoprotein signals had been normalized to their respective total proteins. Data are mean values \pm SEM (* p < 0.05; ** p < 0.01; *** p < 0.001, n = 3).

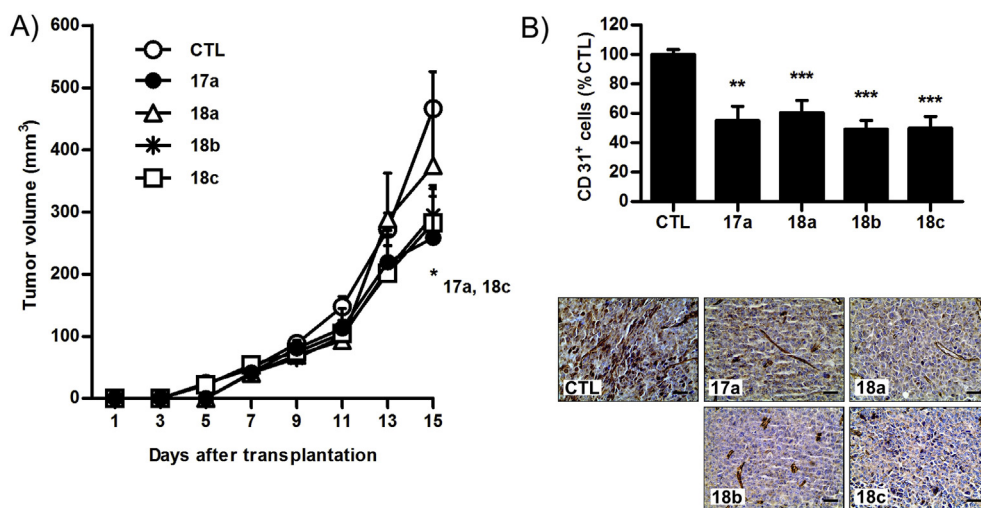


Fig. 4. In vivo effects of **17a** and **18a-c** on LLC tumor growth and vascularization. (A) Tumor volume was evaluated in mice injected with test compounds (0.2 mg/kg of body weight) or DMSO vehicle (CTL). (B) Microvessel density of LLC tumors at end-point as assessed by IHC using CD31 specific antibody. Data represent mean \pm SEM relative to control group (n = 10–17; * p < 0.05). In the lower panel, representative microphotographs (magnification \times 400; scale bar: 50 μ m).

Table 2
Differentially expressed genes by pyrazolopyridines **17a**, **18b-c**.^a

	6 h		24 h	
	Under-expressed	Over-expressed	Under-expressed	Over-expressed
17a	4	10	17	2
18b	2	1	7	7
18c	14	42	112	100

^a Cut-off: p-value < 0.05 & |log₂FC| > 0.5.

recently shown to critically impact the angiogenic process [40–43]. Involvement of VEGFR2 signaling into the observed metabolic changes is also speculated as this pathway has been previously connected with the activation of sterol regulatory element binding proteins (transcription regulators of lipid biosynthesis), an event that is proved to be indispensable for the unobstructed progression of VEGFA-induced angiogenesis [44]. In conclusion, the imposed changes on the gene expression profile of treated HUVEC indicate dysregulation of cell cycle and cholesterol dynamics as two significant mechanisms underlying the angiogenesis modulating action of derivative **18c**. Subsequently, a number of genes, involved in these top deregulated cellular functions (see Supplementary data Tables S4 and S5) were selected to independently confirm, by real-time quantitative reverse PCR (qRT-PCR), the transcriptional changes observed in the microarray experiment. The genes chosen were those encoding for 3-hydroxy-3-methylglutaryl-CoA synthase 1 (*HMGCS1*), methylsterol monooxygenase (*MSMO1*), insulin induced gene 1 (*INSIG1*) squalene epoxidase (*SQLE*), ubiquitin-conjugating enzyme E2C (*UBE2C*), cyclin B2 (*CCNB2*), cyclin A2 (*CCNA2*), cell division cycle 20 (*CDC20*) and heme oxygenase 1

(*HMOX1*). As shown in Fig. 7 for all genes tested the direction and magnitude of changes measured by qRT-PCR were consistent with the results obtained from the microarray analysis.

3. Conclusion

A series of novel pyrazolopyridines were synthesized following a procedure involving the use of a suitable aminopicoline, which upon chemical modifications was ring closed to result in a central pyrazolo[3,4-c]pyridine core, that was successively substituted to provide the target derivatives. Nine compounds were initially evaluated for their activity as inhibitors of EC growth and migration under basal conditions. Subsequently, the anti-angiogenic effects of the best candidates, namely **17a** and **18a-c**, against EC proliferation, migration and differentiation were further demonstrated under VEGF-stimulated conditions. At the level of cell signal transduction the selected inhibitors attenuated VEGF-induced phosphorylation of Tyr-1175 in RTK domain of VEGFR2 and accordingly negatively regulated the VEGF-mediated phosphorylation of downstream kinases AKT and ERK1/2. Moreover, derivatives **17a** and **18b-c** proved to be able to cause in vivo a significant regression of LLC growth and a prominent reduction of tumor microvessel density, without obvious side-effects. Genome-wide microarray profiling and subsequent GO analysis of EC in response to **17a** and **18b-c** identified a commonly targeted cluster of under-expressed genes related to cell division and mitosis and revealed **18c** as the most powerful derivative in inducing gene expression alterations. Additionally, in **18c**-treated EC, cholesterol biosynthesis and lipid metabolism were recognized amongst the top deregulated cellular processes with relevant GO categories mainly comprising over-expressed genes. As

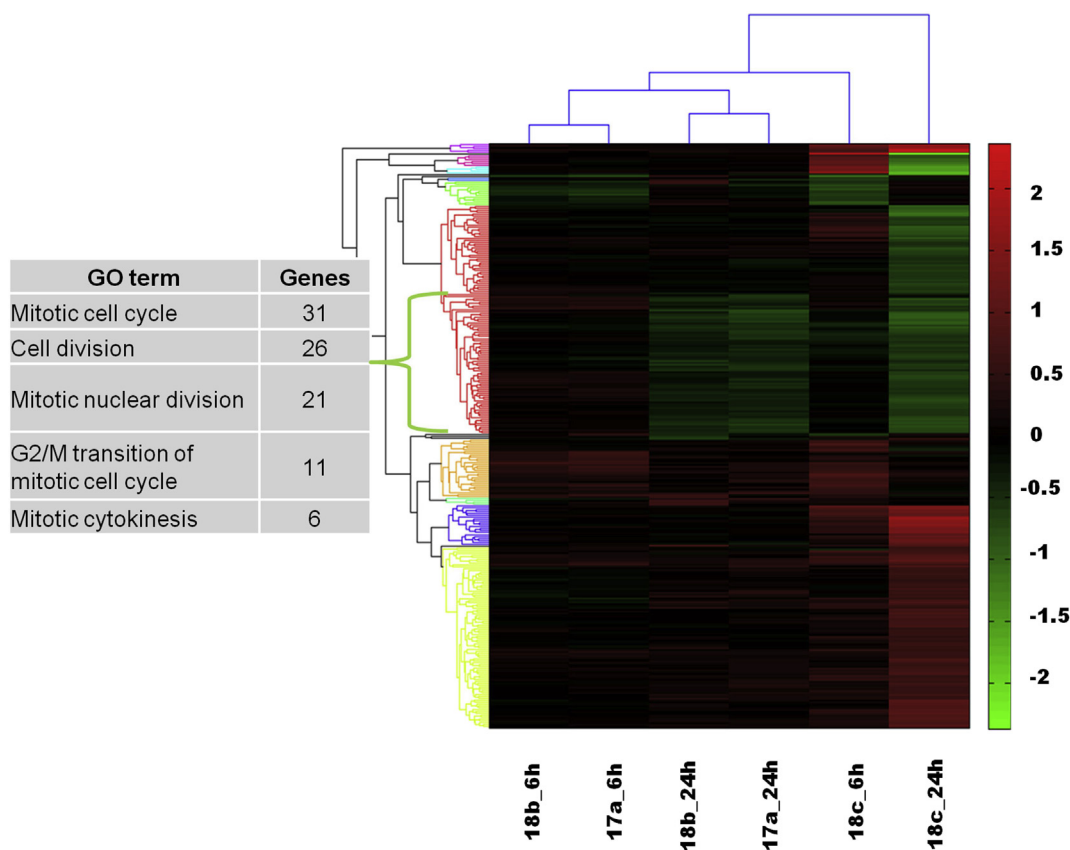


Fig. 5. Hierarchical clustering of the gene expression fold change values (in log₂ scale) in HUVEC treated with compounds **17a**, **18b** and **18c** versus DMSO for 6 h and 24 h. The bracket indicates the top enriched GO terms as indicated by the StRANGER2 analysis, affected by the specific cluster of under-expressed genes common for all compounds at 24 h.

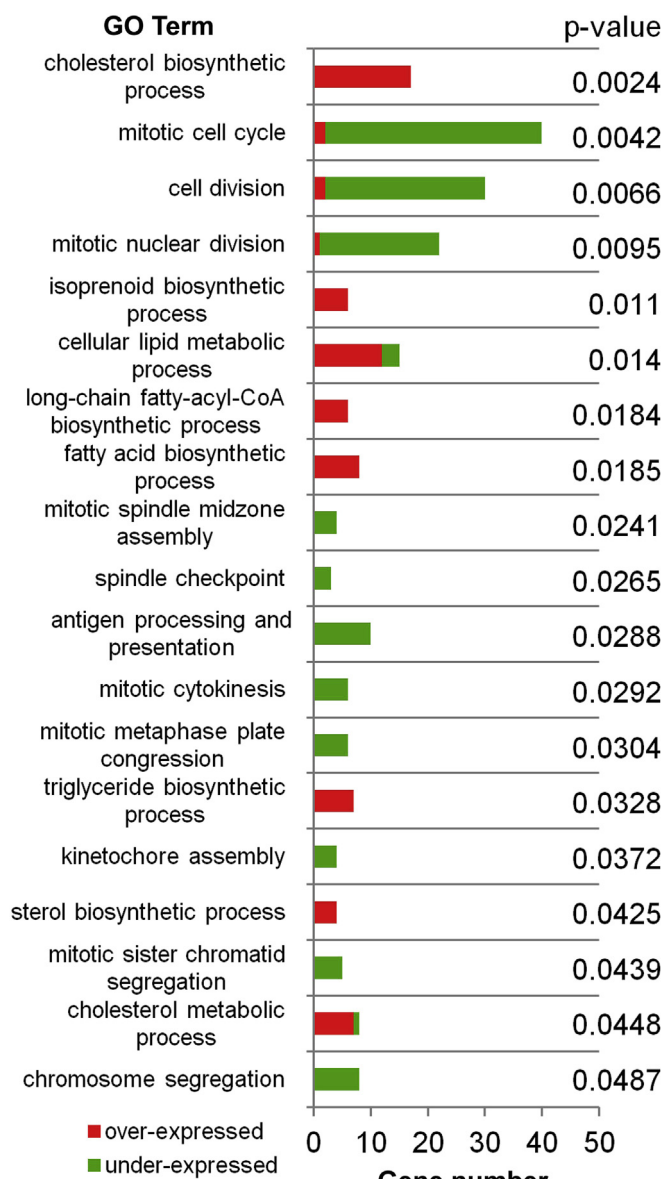


Fig. 6. Bar plot diagram of differentially expressed genes per GO term in HUVEC treated with compound **18c** versus DMSO for 24 h. Functional analysis performed using StrAnGER2 depicts the statistically significant altered biological processes.

far as structure-activity relationships are concerned, a thorough consideration of acquired biological data allowed a preliminary estimation of optimal structural requirements for anti-angiogenic activity. It is noticeable that the best three inhibitors possess a 3-phenyl group, whereas two of the most interesting analogues (**18b** and **18c**) are endowed with a quite similar substitution pattern. Overall, in this study we present convincing preclinical evidence and mechanistic insights into the action of a new type of anti-angiogenic pyrazolopyridines. Our results encourage future assessment of the most promising derivative, **18c**, as a lead for the development of novel agents against angiogenesis-dependent disorders. To this end a detailed structure-activity relationship analysis of new synthesized analogues along with estimation of bioavailability, pharmacokinetics and toxicity profiles would be definitely required.

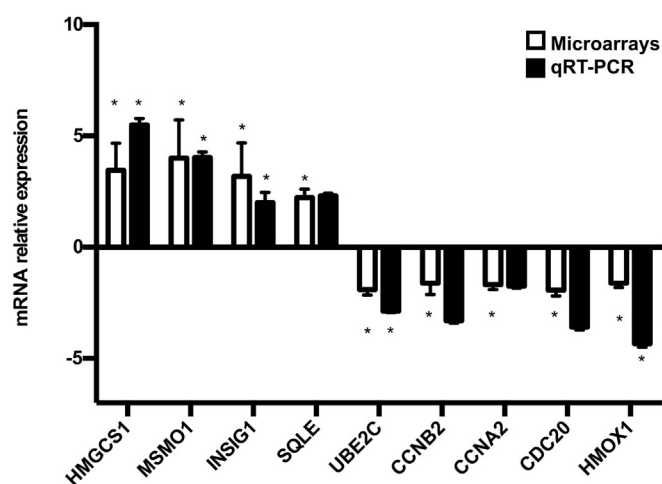


Fig. 7. Validation of microarray data using qRT-PCR in HUVEC treated with compound **18c** or DMSO (control) for 24 h. Relative expression for each gene is shown as fold change versus control. qRT-PCR data represent mean \pm SEM ($n = 3$; * $p < 0.05$).

4. Experimental procedures

4.1. Chemistry

4.1.1. General information

Melting points were determined on a Büchi apparatus and are uncorrected. FT-IR spectra were recorded on a Perkin-Elmer RX1 FT-IR spectrometer. ^1H NMR spectra and 2D spectra were recorded on a Bruker Avance III 600 or a Bruker Avance DRX 400 instrument, whereas ^{13}C NMR spectra were recorded on a Bruker Avance III 600 or a Bruker AC 200 spectrometer in deuterated solvents and were referenced to TMS (δ scale). The signals of ^1H and ^{13}C spectra were unambiguously assigned by using 2D NMR techniques: $^1\text{H}^1\text{H}$ COSY, NOESY, HMQC, and HMBC. Mass spectra were recorded with a LTQ Orbitrap Discovery instrument, possessing an Ionmax ionization source. Flash chromatography was performed on Merck silica gel 60 (0.040–0.063 mm). Analytical thin layer chromatography (TLC) was carried out on precoated (0.25 mm) Merck silica gel F-254 plates. The purity of all the synthesized compounds was $>95\%$ as ascertained by elemental analysis. Elemental analyses were undertaken using a PerkinElmer PE 240C elemental analyzer (Norwalk, CT, U.S.) and the measured values for C, H, and N were within $\pm 0.4\%$ of the theoretical values. Stock solutions of compounds for biological experiments were prepared in DMSO (St. Louis, MO, USA) and stored at -20°C . Working dilutions contained up to 0.1% v/v DMSO.

4.1.2. Synthesis of 5-chloro-1-(4-methoxybenzyl)-1H-pyrazolo[3,4-c]pyridine (**7**)

Sodium hydride (260 mg, 6.52 mmol, 60% in paraffin oil) was added at 0°C , under argon to a solution of the pyrazolopyridine **6** [36] (500 mg, 3.26 mmol) in dry DMF (20 mL) and the reaction mixture was stirred at room temperature for 30 min. The reaction was then cooled to 0°C , a solution of 4-methoxybenzylchloride (0.66 mL, 4.89 mmol) in DMF (2 mL) was added dropwise and the mixture was stirred at room temperature for 2 h. The bulk of the solvent was removed in vacuo, water was added to the residue and it was extracted with dichloromethane (3×50 mL). The organic extracts were dried (Na_2SO_4) and evaporated to dryness to provide both N1 and N2 regio isomers which were separated by column chromatography (silica gel) using a mixture of cyclohexane/ethyl acetate (5/1, v/v) as the eluent.

4.1.2.1. Data for N1-isomer: 5-chloro-1-(4-methoxybenzyl)-1H-pyrazolo[3,4-c]pyridine (7). Yield 57%. Mp 117–119 °C (EtOAc). ¹H NMR (600 MHz, CDCl₃) δ 3.79 (s, 3H, OCH₃), 5.61 (s, 2H, CH₂), 6.87 (d, *J* = 8.5 Hz, 2H, H-3', H-5'), 7.22 (d, *J* = 8.5 Hz, 2H, H-2', H-6'), 7.64 (s, 1H, H-4), 8.03 (s, 1H, H-3), 8.62 (s, 1H, H-7). ¹³C NMR (151 MHz, CDCl₃) δ 53.7, 55.3, 114.4, 115.2, 127.4, 129.0, 131.1, 132.0, 133.2, 135.4, 140.8, 159.7. HR-MS (ESI) *m/z*: Calcd for C₁₄H₁₃N₃OCl: [M1 + H]⁺ = 274.0742, found 274.0746.

4.1.2.2. Data for N2-isomer: 5-chloro-2-(4-methoxybenzyl)-2H-pyrazolo[3,4-c]pyridine. Yield 28%. Mp 92–94 °C (EtOAc). ¹H NMR (600 MHz, CDCl₃) δ 3.81 (s, 3H, OCH₃), 5.58 (s, 2H, CH₂), 6.91 (d, *J* = 8.5 Hz, 2H, H-3', H-5'), 7.30 (d, *J* = 8.5 Hz, 2H, H-2', H-6'), 7.51 (s, 1H, H-4), 7.88 (s, 1H, H-3), 9.07 (s, 1H, H-7). ¹³C NMR (151 MHz, CDCl₃) δ 55.35, 57.99, 112.79, 114.56, 121.96, 126.42, 126.51, 129.96, 140.41, 143.94, 144.58, 160.12.

4.1.3. Synthesis of 5-chloro-1-(4-methoxybenzyl)-1H-pyrazolo[3,4-c]pyridine-6-oxide (8)

3-Chloroperbenzoic acid (1.77 g, 10.24 mmol) was added to a solution of pyrazolopyridine **7** (2 g, 7.31 mmol) in chloroform (120 mL) and the reaction mixture was stirred at room temperature, away from light, for three days. Upon completion of the reaction, the solvent was evaporated and a solution of sodium carbonate (150 mL, 5% w/v) was added to the residue. The white precipitate was filtered under vacuum, washed with a small quantity of water (10 mL) and air-dried, to provide 1.9 g of pure *N*-oxide **8**. Yield 90%. Mp 156–8 °C (EtOH). IR (Nujol) ν 1612, 1585, 1514, 1245, 1177, 1143, 1062, 1024, 797 cm⁻¹. ¹H NMR (400 MHz, methanol-*d*₄) δ 3.80 (s, 3H, OCH₃), 5.47 (s, 2H, CH₂), 6.87 (d, 2H, *J* = 8.0 Hz, H-3', H-5'), 7.20 (d, 2H, *J* = 8.0 Hz, H-2', H-6'), 7.83 (s, 1H, H-4), 7.99 (s, 1H, H-3), 8.58 (s, 1H, H-7). ¹³C NMR (50 MHz, methanol-*d*₄) δ 52.3, 55.5, 114.4, 118.1, 120.3, 123.9, 128.8, 129.8, 133.7, 134.8, 135.7, 159.3. Anal. Calcd for C₁₄H₁₂ClN₃O₂: C, 58.04; H, 4.17; N, 14.50. Found: C, 57.96; H, 4.21; N, 14.43.

4.1.4. Synthesis of 5,7-dichloro-1-(4-methoxybenzyl)-1H-pyrazolo[3,4-c]pyridine (9)

Phosphorous oxychloride (2.2 mL, 24.35 mmol) was added dropwise, at 0 °C, to a solution of the *N*-oxide **8** (1.5 g, 4.87 mmol) in dry tetrahydrofuran (20 mL) and the reaction mixture was stirred at room temperature for 12 h. Then, it was poured into crushed ice (100 mL), made alkaline with a solution of sodium carbonate (5% w/v) and extracted with dichloromethane (3 × 100 mL). The combined organic layers were dried (Na₂SO₄) and evaporated to dryness. The crude product was purified by column chromatography (silica gel) using a mixture of cyclohexane/ethyl acetate (75/25, v/v) as the eluent, to provide 1.4 g of the dichloro compound **9**. Yield 93%. Mp 101–3 °C (Et₂O/*n*-hexane). IR (Nujol) ν 1605, 1582, 1507, 1245, 1174, 1096, 1028, 797 cm⁻¹. ¹H NMR (600 MHz, CDCl₃) δ 3.79 (s, 3H, OCH₃), 5.92 (s, 2H, CH₂), 6.85 (d, 2H, *J* = 8.5 Hz, H-3', H-5'), 7.20 (d, 2H, *J* = 8.5 Hz, H-2', H-6'), 7.59 (s, 1H, H-4), 8.09 (s, 1H, H-3). ¹³C NMR (151 MHz, CDCl₃) δ 53.9, 55.2, 114.0, 114.1, 128.6, 128.6, 132.3, 132.4, 132.7, 133.1, 138.6, 159.3. HR-MS (ESI) *m/z*: Calcd for C₁₄H₁₂Cl₂N₃O: [M1 + H]⁺ = 308.0352, found 308.0355. Anal. Calcd for C₁₄H₁₁Cl₂N₃O: C, 54.57; H, 3.60; N, 13.64. Found: C, 54.43; H, 3.51; N, 13.79.

4.1.5. Synthesis of 5-chloro-1-(4-methoxybenzyl)-7-(piperazin-1-yl)-1H-pyrazolo[3,4-c]pyridine (10a)

A mixture of compound **9** (200 mg, 0.65 mmol) and piperazine (560 mg, 6.5 mmol) was irradiated at 160 °C (300 W, Milestone Start E) for 3 min. Upon cooling the mixture was poured into water (100 mL) and extracted with dichloromethane (3 × 50 mL). The crude product was purified by column chromatography (silica gel)

using a mixture of dichloromethane/methanol (from 100/5 up to 100/12, v/v) as the eluent. Yield: 82%. Mp 77–79 °C (CH₂Cl₂/Et₂O). IR (Nujol) ν 3242, 1612, 1585, 1558, 1510, 1310, 1266, 1245, 1174, 1085, 1028, 803, 732 cm⁻¹. ¹H NMR (400 MHz, CDCl₃) δ 2.96 (m, 4H, piperazine H), 3.14 (m, 4H, piperazine H), 3.59 (s, 3H, OCH₃), 5.59 (s, 2H, CH₂), 6.67 (d, 2H, *J* = 8.6 Hz, H-3', H-5'), 7.00 (d, 2H, *J* = 8.6 Hz, H-2', H-6'), 7.11 (s, 1H, H-4), 7.85 (s, 1H, H-3). ¹³C NMR (50 MHz, CDCl₃) δ 45.4, 49.8, 51.7, 55.0, 109.3, 113.9, 128.4, 129.0, 129.4, 133.0, 133.7, 138.4, 148.9, 159.0. HR-MS (ESI) *m/z*: Calcd for C₁₈H₂₁ClN₅O: [M1 + H]⁺ = 358.1429, found 358.1434. Anal. Calcd for C₁₈H₂₀ClN₅O: C, 60.42; H, 5.63; N, 19.57. Found: C, 60.74; H, 5.46; N, 19.77.

4.1.6. Synthesis of 5-chloro-1-(4-methoxybenzyl)-7-(4-methylpiperazin-1-yl)-1H-pyrazolo[3,4-c]pyridine (10b)

A mixture of compound **9** (988 mg, 3.21 mmol) and 1-methylpiperazine (3.2 g, 31.9 mmol) was refluxed for 20 min, under argon. The mixture was then poured into water (200 mL) and extracted with dichloromethane (3 × 100 mL). The crude product was purified by column chromatography (silica gel) using a mixture of dichloromethane/methanol (from 100/5 up to 100/10, v/v) as the eluent to provide pure **10b** as an oil. Yield: 89%. IR (film) ν 2955, 2921, 2860, 1602, 1558, 1514, 1459, 1249, 1167, 1085, 1028, 798 cm⁻¹. ¹H NMR (400 MHz, CDCl₃) δ 2.28 (s, 3H, CH₃-piperazine), 2.66 (m, 4H, piperazine H), 3.35 (m, 4H, piperazine H), 3.72 (s, 3H, OCH₃), 5.69 (s, 2H, CH₂), 6.79 (d, 2H, *J* = 8.6 Hz, H-3', H-5'), 7.15 (d, 2H, *J* = 8.6 Hz, H-2', H-6'), 7.21 (s, 1H, H-4), 7.95 (s, 1H, H-3). ¹³C NMR (50 MHz, CDCl₃) δ 46.1, 50.4, 53.0, 54.6, 55.0, 108.9, 113.8, 128.6, 129.0, 129.4, 132.9, 133.8, 138.4, 148.6, 158.9. HR-MS (ESI) *m/z*: Calcd for C₁₉H₂₃ClN₅O: [M1 + H]⁺ = 372.1586, found 372.1589. Anal. Calcd for C₁₉H₂₂ClN₅O: C, 61.37; H, 5.96; N, 18.83. Found: C, 61.45; H, 5.99; N, 18.96.

4.1.7. Synthesis of 5-chloro-1-(4-methoxybenzyl)-7-(pyrrolidin-1-yl)-1H-pyrazolo[3,4-c]pyridine (10c)

This compound was prepared by a procedure analogous to that of **10a**. Purification was effected by column chromatography (silica gel) using a mixture of cyclohexane/ethyl acetate (from 90/10 up to 70/30, v/v) as the eluent to provide pure **10c** as an oil. Yield: 91%. IR (film) ν 2954, 2922, 2873, 1612, 1562, 1513, 1458, 1248, 1175, 1074, 1033, 797 cm⁻¹. ¹H NMR (400 MHz, CDCl₃) δ 1.95 (m, 4H, pyrrolidine H), 3.53 (m, 4H, pyrrolidine H), 3.74 (s, 3H, OCH₃), 5.63 (s, 2H, CH₂), 6.78 (d, 2H, *J* = 8.6 Hz, H-3', H-5'), 7.07 (d, 2H, *J* = 8.6 Hz, H-2', H-6'), 7.10 (s, 1H, H-4), 7.92 (s, 1H, H-3). ¹³C NMR (50 MHz, CDCl₃) δ 24.8, 51.1, 53.9, 55.2, 107.0, 114.0, 128.7, 129.2, 130.2, 132.9, 134.0, 138.5, 148.1, 159.1. HR-MS (ESI) *m/z*: Calcd for C₁₈H₂₀ClN₄O: [M1 + H]⁺ = 343.1320, found 343.1326. Anal. Calcd for C₁₈H₁₉ClN₄O: C, 63.06; H, 5.59; N, 16.34. Found: C, 63.26; H, 5.70; N, 16.16.

4.1.8. General procedure for the synthesis of 5,7-bis substituted 1-(4-methoxybenzyl)-1H-pyrazolo[3,4-c]pyridines 11a–d

Aniline (0.164 mL, 1.8 mmol) or 4-(4-methylpiperazin-1-yl)aniline (210 mg, 1.1 mmol) was added under argon to a solution of the 7-aminosubstituted-5-chloro-pyrazolopyridines **10a–c** (1 mmol) in dry toluene (25 mL), followed by addition of cesium carbonate (1.3 g, 4 mmol), 2-dicyclohexylphosphino-2',4',6'-triisopropylbiphenyl (*X*-phos, 24 mg, 0.05 mmol) and bis(dibenzylideneacetone) palladium(0) (29 mg, 0.05 mmol) and the resulting mixture was refluxed for 18 h. Upon completion of reaction, the mixture was filtered through a celite pad, the filtrate was vacuum-evaporated, extracted with ethyl acetate – water and the extracts were dried and evaporated to dryness. The crude product was then purified by column chromatography (silica gel) to provide pure compounds **11a–d**.

4.1.8.1. 1-(4-Methoxybenzyl)-N-phenyl-7-(piperazin-1-yl)-1H-pyrazolo[3,4-c]pyridin-5-amine (11a). This compound was prepared according to the general procedure described above. Purification was effected using a mixture of dichloromethane/methanol (from 100/5 up to 100/14, v/v) as the eluent. Yield: 79%. Mp 131–132 °C (EtOAc/*n*-pentane). IR (Nujol) ν 3264, 3169, 1608, 1571, 1518, 1250, 1232, 1170, 1033, 812, 730 cm^{-1} . ^1H NMR (600 MHz, methanol- d_4) δ 3.04 (m, 4H, piperazine H), 3.25 (m, 4H, piperazine H), 3.71 (s, 3H, OCH₃), 5.68 (s, 2H, CH₂), 6.77 (s, 1H, H-4), 6.79 (d, 2H, J = 8.6 Hz, H-3', H-5'), 6.84 (m, 1H, H-4''), 7.07 (d, 2H, J = 8.7 Hz, H-2', H-6'), 7.22 (t, 2H, J = 7.2 Hz, H-3'', H-5''), 7.41 (d, 2H, J = 7.4 Hz, H-2'', H-6''), 7.89 (s, 1H, H-3). ^{13}C NMR (151 MHz, methanol- d_4) δ 46.4, 52.6, 54.1, 55.8, 93.1, 115.0, 119.0, 121.3, 127.7, 129.5, 129.9, 131.5, 134.6, 135.6, 144.5, 149.5, 149.8, 160.7. HR-MS (ESI) m/z : Calcd for C₂₄H₂₇N₆O: [M + H]⁺ = 415.2241, found 415.2242. Anal. Calcd for C₂₄H₂₆N₆O: C, 69.54; H, 6.32; N, 20.27. Found: C, 69.77; H, 6.20; N, 20.53.

4.1.8.2. 1-(4-Methoxybenzyl)-7-(4-methylpiperazin-1-yl)-N-phenyl-1H-pyrazolo[3,4-c]pyridin-5-amine (11b). This compound was prepared according to the general procedure described above. Purification was effected using a mixture of dichloromethane/methanol (from 100/2 up to 100/8, v/v) as the eluent. Yield: 77%. Mp 117–118 °C (Et₂O/*n*-pentane). IR (Nujol) ν 3167, 1599, 1565, 1510, 1262, 1238, 1170, 1143, 1031, 1007, 848, 732 cm^{-1} . ^1H NMR (600 MHz, CDCl₃) δ 2.81 (s, 3H, CH₃-piperazine), 3.14 (brs, 2H, piperazine H), 3.37 (brs, 2H, piperazine H), 3.70 (brs, 2H, piperazine H), 3.75 (s, 3H, OCH₃), 3.99 (brs, 2H, piperazine H), 5.57 (s, 2H, CH₂), 6.28 (brs, 1H, NH-aniline, D₂O exch), 6.78 (d, 2H, J = 8.6 Hz, H-3', H-5'), 6.87 (s, 1H, H-4), 7.00–7.07 (m, 3H, H-4'', H-2', H-6'), 7.22 (d, 2H, J = 7.6 Hz, H-2'', H-6''), 7.31 (t, 2H, J = 7.6 Hz, H-3'', H-5''), 7.88 (s, 1H, H-3). ^{13}C NMR (50 MHz, CDCl₃) δ 46.3, 50.5, 53.0, 55.0, 55.3, 90.9, 114.0, 118.5, 121.3, 126.8, 128.8, 129.2, 129.8, 133.7, 133.8, 142.2, 147.3, 148.2, 159.0. HR-MS (ESI) m/z : Calcd for C₂₅H₂₉N₆O: [M + H]⁺ = 429.2397, found 429.2402. Anal. Calcd for C₂₅H₂₈N₆O: C, 70.07; H, 6.59; N, 19.61. Found: C, 69.98; H, 6.47; N, 19.69.

4.1.8.3. 1-(4-Methoxybenzyl)-7-(4-methylpiperazin-1-yl)-N-(4-(4-methylpiperazin-1-yl)phenyl)-1H-pyrazolo[3,4-c]pyridin-5-amine (11c). This compound was prepared according to the general procedure described above. Purification was effected using a mixture of dichloromethane/methanol (from 100/1 up to 100/5, v/v) as the eluent. Yield: 88%. Mp 136–138 °C (Et₂O/*n*-pentane). IR (Nujol) ν 3392, 3283, 1605, 1568, 1514, 1245, 1174, 1143, 1031, 1004, 817, 722 cm^{-1} . ^1H NMR (600 MHz, methanol- d_4) δ 2.43 (s, 3H, CH₃-piperazine), 2.44 (s, 3H, CH₃-piperazine), 2.75 (m, 8H, piperazine H), 3.16 (m, 4H, piperazine H), 3.32 (m, 4H, piperazine H, overlapping with methanol- d_4), 3.72 (s, 3H, OCH₃), 5.65 (s, 2H, CH₂), 6.66 (s, 1H, H-4), 6.79 (d, 2H, J = 8.7 Hz, H-3', H-5'), 6.95 (d, 2H, J = 8.9 Hz, H-3'', H-5''), 7.06 (d, 2H, J = 8.6 Hz, H-2', H-6'), 7.33 (d, 2H, J = 8.6 Hz, H-2'', H-6''), 7.86 (s, 1H, H-3). ^{13}C NMR (151 MHz, methanol- d_4) δ 45.9, 46.2, 51.3, 51.4, 54.1, 55.8, 55.9, 56.1, 115.0, 115.1, 119.2, 121.2, 129.5, 129.7, 131.5, 134.5, 138.2, 146.8, 149.0, 160.7. HR-MS (ESI) m/z : Calcd for C₃₀H₃₉N₈O: [M + H]⁺ = 527.3241, found 527.3243. Anal. Calcd for C₃₀H₃₈N₈O: C, 68.41; H, 7.27; N, 21.28. Found: C, 68.30; H, 7.44; N, 21.49.

4.1.8.4. 1-(4-Methoxybenzyl)-N-(4-(4-methylpiperazin-1-yl)phenyl)-7-(pyrrolidin-1-yl)-1H-pyrazolo[3,4-c]pyridin-5-amine (11d). This compound was prepared according to the general procedure described above. Purification was effected using a mixture of dichloromethane/methanol (from 100/2 up to 100/10, v/v) as the eluent. Yield: 83%. Mp 122–124 °C (Et₂O/*n*-pentane). IR (Nujol) ν 3392, 1605, 1568, 1517, 1293, 1245, 1174, 1143, 1031, 1004, 926, 814, 725 cm^{-1} . ^1H NMR (400 MHz, CDCl₃) δ 1.93 (m, 4H, pyrrolidine H), 2.35 (s, 3H, CH₃-piperazine), 2.59 (m, 4H, piperazine H), 3.17 (m, 4H,

piperazine H), 3.48 (m, 4H, pyrrolidine H), 3.71 (s, 3H, OCH₃), 5.57 (s, 2H, CH₂), 6.11 (brs, 1H, NH-aniline, D₂O exch), 6.47 (s, 1H, H-4), 6.76 (d, 2H, J = 8.7 Hz, H-3', H-5'), 6.90 (d, 2H, J = 8.9 Hz, H-3'', H-5''), 7.11 (d, 2H, J = 8.7 Hz, H-2', H-6'), 7.18 (d, 2H, J = 8.9 Hz, H-2'', H-6''), 7.76 (s, 1H, H-3). ^{13}C NMR (50 MHz, CDCl₃) δ 24.6, 46.1, 49.9, 50.8, 53.6, 55.2, 87.3, 113.9, 117.4, 121.9, 127.3, 128.8, 129.9, 133.7, 133.8, 134.8, 146.8, 147.5, 148.8, 158.9. HR-MS (ESI) m/z : Calcd for C₂₉H₃₆N₇O: [M + H]⁺ = 498.2976, found 498.2979. Anal. Calcd for C₂₉H₃₅N₇O: C, 69.99; H, 7.09; N, 19.70. Found: C, 70.23; H, 7.22; N, 19.61.

4.1.9. Synthesis of 5-chloro-1-(4-methoxybenzyl)-3-phenyl-1H-pyrazolo[3,4-c]pyridine (14)

Phenylboronic acid (416 mg, 3.42 mmol) and palladium(0) tetrakis(triphenylphosphine) (180 mg, 0.15 mmol) were added to a solution of the iodo compound **13** (1.24 g, 3.1 mmol) in a mixture of toluene (100 mL) and ethanol (10 mL), followed by addition of an aqueous solution (2 mL) of sodium hydrogen carbonate (780 mg, 9.30 mmol) and the resulting mixture was refluxed for 16 h. The solvents were then vacuum-evaporated, the residue was extracted with dichloromethane – water, and the combined extracts were dried (Na₂SO₄) and evaporated to dryness. The crude mixture was purified by column chromatography (silica gel), using a mixture of dichloromethane/ethyl acetate (99/1, v/v) as the eluent, to provide pure **14** (1.08 g, yield 100%). Mp 73–75 °C (MeOH). ^1H NMR (400 MHz, CDCl₃) δ 3.71 (s, 3H, OCH₃), 5.56 (s, 2H, CH₂), 6.83 (d, 2H, H-2', H-6', J = 8.5 Hz), 7.23 (d, 2H, H-3', H-5', J = 8.5 Hz), 7.40 (t, 1H, H-4'', J = 7.5 Hz), 7.49 (t, 2H, H-3'', H-5'', J = 7.5 Hz), 7.83 (s, 1H, H-4), 7.91 (d, 2H, H-2'', H-6'', J = 7.5 Hz), 8.58 (s, 1H, H-7). ^{13}C NMR (50 MHz, CDCl₃) δ 53.5, 55.0, 114.1, 114.5, 126.8, 127.3, 128.3, 128.4, 128.8, 129.0, 131.8, 133.3, 136.5, 141.1, 142.8, 159.4. HR-MS (ESI) m/z : Calcd for C₂₀H₁₇ClN₃O: [M + H]⁺ = 350.1055, found 350.1061. Anal. Calcd for C₂₀H₁₆ClN₃O: C, 68.67; H, 4.61; N, 12.01. Found: C, 68.44; H, 4.49; N, 11.87.

4.1.10. Synthesis of 5-chloro-1-(4-methoxybenzyl)-3-phenyl-1H-pyrazolo[3,4-c]pyridine-6-oxide (15)

This compound was prepared by a procedure analogous to that of **8**. The crude product was purified by column chromatography (silica gel), using a mixture of cyclohexane/ethyl acetate (from 80/20 up to 0/100, v/v) as the eluent, to provide **15** (420 mg, yield 57%). Mp 142–144 °C (EtOH). IR (Nujol) ν 1609, 1585, 1514, 1249, 1174, 1136, 1068, 1028, 722 cm^{-1} . ^1H NMR (400 MHz, CDCl₃) δ 3.73 (s, 3H, OCH₃), 5.46 (s, 2H, CH₂), 6.81 (d, 2H, H-2', H-6', J = 8.7 Hz), 7.21 (d, 2H, H-3', H-5', J = 8.7 Hz), 7.40 (t, 1H, H-4'', J = 7.4 Hz), 7.48 (t, 2H, H-3'', H-5'', J = 7.4 Hz), 7.83 (d, 2H, H-2'', H-6'', J = 7.8 Hz), 7.99 (s, 1H, H-4), 8.58 (s, 1H, H-7). ^{13}C NMR (50 MHz, CDCl₃) δ 53.9, 55.3, 114.5, 117.4, 119.1, 123.6, 126.7, 127.1, 129.0, 129.1, 129.2, 131.2, 136.1, 136.5, 144.0, 159.8. Anal. Calcd for C₂₀H₁₆ClN₃O₂: C, 65.67; H, 4.41; N, 11.49. Found: C, 65.86; H, 4.57; N, 11.12.

4.1.11. Synthesis of 5,7-dichloro-1-(4-methoxybenzyl)-3-phenyl-1H-pyrazolo[3,4-c]pyridine (16)

This compound was prepared by a procedure analogous to that of **9**. The crude product was purified by column chromatography (silica gel), using a mixture of cyclohexane/ethyl acetate (90/10, v/v) as the eluent, to provide pure **16** (3.2 g, yield 84%). Mp 126–127 °C (Et₂O/*n*-hexane). IR (Nujol) ν 1612, 1584, 1510, 1266, 1247, 1147, 1024, 722 cm^{-1} . ^1H NMR (400 MHz, CDCl₃) δ 3.76 (s, 3H, OCH₃), 5.95 (s, 2H, CH₂), 6.83 (d, 2H, H-2', H-6', J = 8.7 Hz), 7.24 (d, 2H, H-3', H-5', J = 8.7 Hz), 7.45 (t, 1H, H-4'', J = 7.6 Hz), 7.52 (t, 2H, H-3'', H-5'', J = 7.7 Hz), 7.83 (s, 1H, H-4), 7.87 (d, 2H, H-2'', H-6'', J = 7.6 Hz), ^{13}C NMR (50 MHz, CDCl₃) δ 54.1, 55.3, 114.2, 114.4, 127.4, 128.8, 128.9, 129.1, 129.2, 131.0, 131.5, 132.7, 133.9, 139.2, 144.1, 159.4. HR-MS (ESI) m/z : Calcd for C₂₀H₁₆Cl₂N₃O: [M + H]⁺ = 384.0665,

found 384.0669. Anal. Calcd for $C_{20}H_{15}Cl_2N_3O$: C, 62.51; H, 3.93; N, 10.94. Found: C, 62.39; H, 3.99; N, 11.21.

4.1.12. Synthesis of 5-chloro-1-(4-methoxybenzyl)-3-phenyl-7-(piperazin-1-yl)-1H-pyrazolo[3,4-c]pyridine (**17a**)

This compound was prepared by a procedure analogous to that of **10a**. It was purified by column chromatography using a mixture of dichloromethane/methanol (from 100/2 up to 100/10, v/v) as the eluent. Yield: 91%. Mp 127–129 °C (EtOAc/n-pentane). IR (Nujol) ν 3378, 3180, 1609, 1582, 1544, 1510, 1286, 1249, 1174, 1113, 1072, 1021, 939, 810, 695 cm^{-1} . 1H NMR (400 MHz, $CDCl_3$) δ 3.17 (m, 4H, piperazine H), 3.36 (m, 4H, piperazine H), 3.74 (s, 3H, OCH_3), 5.74 (s, 2H, CH_2), 6.79 (d, 2H, $J = 8.7$ Hz, H-3', H-5'), 7.17 (d, 2H, $J = 8.7$ Hz, H-2', H-6'), 7.42 (t, 1H, $J = 7.4$ Hz, H-4''), 7.50 (t, 2H, $J = 7.5$ Hz, H-3'', H-5''), 7.55 (s, 1H, H-4), 7.87 (d, 2H, $J = 7.4$ Hz, H-2'', H-6''). ^{13}C NMR (50 MHz, $CDCl_3$) δ 45.3, 51.5, 53.4, 55.4, 109.9, 114.1, 127.4, 128.6, 128.7, 129.1, 129.3, 131.0, 131.1, 132.4, 139.3, 145.1, 159.2. HR-MS (ESI) m/z : Calcd for $C_{24}H_{25}ClN_5O$: $[M + H]^+ = 434.1742$, found 434.1746. Anal. Calcd for $C_{24}H_{24}ClN_5O$: C, 66.43; H, 5.57; N, 16.14. Found: C, 66.68; H, 5.77; N, 16.01.

4.1.13. Synthesis of 5-chloro-1-(4-methoxybenzyl)-3-phenyl-7-(4-methylpiperazin-1-yl)-1H-pyrazolo[3,4-c]pyridine (**17b**)

This compound was prepared by a procedure analogous to that of **10a**. It was purified by column chromatography using a mixture of dichloromethane/methanol (from 100/1 up to 100/8, v/v) as the eluent to provide pure **17b** as foam. Yield: 89%. IR (film) ν 3044, 2941, 2839, 2798, 1609, 1585, 1554, 1510, 1463, 1266, 1177, 1031, 820 cm^{-1} . 1H NMR (400 MHz, $CDCl_3$) δ 2.39 (s, 3H, CH_3 -piperazine), 2.66 (m, 4H, piperazine H), 3.38 (m, 4H, piperazine H), 3.70 (s, 3H, OCH_3), 5.73 (s, 2H, CH_2), 6.79 (d, 2H, $J = 8.6$ Hz, H-3', H-5'), 7.21 (d, 2H, $J = 8.6$ Hz, H-2', H-6'), 7.35–7.50 (m, 3H, H-3'', H-4'', H-5''), 7.54 (s, 1H, H-4), 7.88 (d, 2H, $J = 7.0$ Hz, H-2'', H-6''). ^{13}C NMR (50 MHz, $CDCl_3$) δ 46.1, 50.5, 53.1, 54.7, 55.1, 109.3, 113.8, 127.2, 128.4, 128.6, 128.8, 129.1, 130.7, 132.2, 139.1, 144.8, 148.9, 159.0. HR-MS (ESI) m/z : Calcd for $C_{25}H_{27}ClN_5O$: $[M + H]^+ = 448.1899$, found 448.1901. Anal. Calcd for $C_{25}H_{26}ClN_5O$: C, 67.03; H, 5.85; N, 15.63. Found: C, 66.96; H, 5.89; N, 15.52.

4.1.14. Synthesis of 1-(4-methoxybenzyl)-N,3-diphenyl-7-(piperazin-1-yl)-1H-pyrazolo[3,4-c]pyridin-5-amine (**18a**)

This compound was prepared according to the general procedure described above for compounds **11a–d**. It was purified by column chromatography using a mixture of dichloromethane/methanol (from 100/2 up to 100/8, v/v) as the eluent. Yield: 73%. Mp 142–143 °C (EtOAc). IR (Nujol) ν 3399, 3174, 1599, 1561, 1514, 1245, 1174, 1028, 905, 810, 752, 695 cm^{-1} . 1H NMR (600 MHz, methanol- d_4) δ 3.18 (m, 4H, piperazine H), 3.36 (brs, 4H, piperazine H), 3.71 (s, 3H, OCH_3), 5.73 (s, 2H, CH_2), 6.82 (d, 2H, $J = 8.7$ Hz, H-3', H-5'), 6.86 (m, 1H, H-4'''), 7.06 (s, 1H, H-4), 7.14 (d, 2H, $J = 8.7$ Hz, H-2', H-6'), 7.23 (t, 2H, $J = 7.2$ Hz, H-3'', H-5''), 7.38 (t, 1H, $J = 7.4$ Hz, H-4''), 7.44–7.50 (m, 4H, H-3'', H-5'', H-2'', H-6'''), 7.86 (d, 2H, $J = 7.4$ Hz, H-2'', H-6''). ^{13}C NMR (151 MHz, methanol- d_4) δ 45.8, 51.4, 54.4, 55.8, 93.8, 115.1, 119.1, 121.4, 128.3, 128.8, 129.4, 129.5, 129.9, 130.1, 131.5, 133.2, 134.4, 144.4, 145.4, 149.1, 150.5, 160.8. HR-MS (ESI) m/z : Calcd for $C_{30}H_{31}N_6O$: $[M + H]^+ = 491.2554$, found 491.2557. Anal. Calcd for $C_{30}H_{30}N_6O$: C, 73.45; H, 6.16; N, 17.13. Found: C, 73.21; H, 6.01; N, 17.33.

4.1.15. Synthesis of 1-(4-methoxybenzyl)-N-(4-(4-methylpiperazin-1-yl)phenyl)-3-phenyl-7-(piperazin-1-yl)-1H-pyrazolo[3,4-c]pyridin-5-amine (**18b**)

This compound was prepared according to the general procedure described above for compounds **11a–d**. It was purified by column chromatography using a mixture of dichloromethane/

methanol (from 100/4 up to 100/12, v/v) as the eluent. Yield: 68%. Mp 217–218 °C (EtOAc). IR (Nujol) ν 3290, 3187, 1626, 1534, 1510, 1269, 1249, 1170, 1143, 1109, 1031, 902, 807, 722 cm^{-1} . 1H NMR (600 MHz, methanol- d_4) δ 2.35 (s, 3H, CH_3 -piperazine), 2.63 (m, 4H, piperazine H), 3.08 (m, 4H, piperazine H), 3.13 (m, 4H, piperazine H), 3.29 (brs, 4H, piperazine H), 3.71 (s, 3H, OCH_3), 5.72 (s, 2H, CH_2), 6.80 (d, 2H, $J = 8.7$ Hz, H-3', H-5'), 6.92 (s, 1H, H-4), 6.95 (d, 2H, $J = 8.9$ Hz, H-3''', H-5'''), 7.15 (d, 2H, $J = 8.7$ Hz, H-2', H-6'), 7.38 (m, 3H, H-4'', H-2''', H-6'''), 7.47 (t, 2H, $J = 7.6$ Hz, H-3'', H-5''), 7.83 (d, 2H, $J = 7.4$ Hz, H-2'', H-6''). ^{13}C NMR (151 MHz, methanol- d_4) δ 46.2, 46.4, 51.5, 52.4, 54.3, 55.8, 56.2, 91.9, 115.0, 119.1, 121.1, 128.2, 128.7, 129.3, 129.6, 130.0, 131.5, 133.2, 134.6, 138.1, 145.3, 147.0, 149.8, 151.4, 160.7. HR-MS (ESI) m/z : Calcd for $C_{35}H_{41}N_8O$: $[M + H]^+ = 589.3398$, found 589.3405. Anal. Calcd for $C_{35}H_{40}N_8O$: C, 71.40; H, 6.85; N, 19.03. Found: C, 71.61; H, 6.99; N, 18.92.

4.1.16. Synthesis of 1-(4-methoxybenzyl)-7-(4-methylpiperazin-1-yl)-N-(4-(4-methylpiperazin-1-yl)phenyl)-3-phenyl-1H-pyrazolo[3,4-c]pyridin-5-amine (**18c**)

This compound was prepared according to the general procedure described above for compounds **11a–d**. It was purified by column chromatography using a mixture of dichloromethane/methanol (from 100/3 up to 100/10, v/v) as the eluent. Yield: 80%. Mp 161–162 °C (Et₂O/n-pentane). IR (Nujol) ν 3324, 3174, 1602, 1577, 1554, 1514, 1303, 1252, 1174, 1147, 1011, 817, 723 cm^{-1} . 1H NMR (400 MHz, $CDCl_3$) δ 2.36 (s, 3H, CH_3 -piperazine), 2.40 (s, 3H, CH_3 -piperazine), 2.61 (m, 4H, piperazine H), 2.67 (brs, 4H, piperazine H), 3.17 (m, 4H, piperazine H), 3.34 (brs, 4H, piperazine H), 3.73 (s, 3H, OCH_3), 5.68 (s, 2H, CH_2), 6.21 (brs, 1H, D₂O exch, NH), 6.77 (d, 2H, $J = 8.6$ Hz, H-3', H-5'), 6.90–6.94 (m, 3H, H-4, H-3''', H-5'''), 7.18–7.24 (m, 4H, H-2', H-6', H-2''', H-6'''), 7.34 (t, 1H, $J = 7.3$ Hz, H-4''), 7.43 (t, 2H, $J = 7.4$ Hz, H-3'', H-5''), 7.83 (d, 2H, $J = 7.4$ Hz, H-2'', H-6''). ^{13}C NMR (50 MHz, $CDCl_3$) δ 46.2, 46.3, 49.9, 50.5, 53.1, 55.1, 55.3, 89.5, 113.9, 117.5, 121.2, 127.1, 127.7, 127.8, 128.8, 130.0, 131.7, 133.5, 134.8, 144.1, 146.7, 148.5, 149.3, 158.9. HR-MS (ESI) m/z : Calcd for $C_{36}H_{43}N_8O$: $[M + H]^+ = 603.3554$, found 603.3558. Anal. Calcd for $C_{36}H_{42}N_8O$: C, 71.73; H, 7.02; N, 18.59. Found: C, 71.87; H, 7.00; N, 18.39.

4.2. Biological studies

4.2.1. Cell culture

EA.hy926 immortalized human EC (kindly provided by Prof. A. Papapetropoulos, National and Kapodistrian University of Athens), were maintained in DMEM containing 10% FBS, 1% L-glutamine, 2% hypoxanthine-aminopterin-thymidine mixture and antibiotics (10 U/mL penicillin, 100 mg/mL streptomycin). HUVEC were isolated from the vein of fresh umbilical cords, collected from 3 to 5 donors, following collagenase digestion as previously described [45] and maintained in pooled cultures up to passage 4 in M199 including 15% FBS, 1% L-glutamine, 5 U/mL heparin, 0.2 mg/mL ECGS and antibiotics. HUVEC identification was regularly certified from typical cobblestone cell morphology and the presence of endothelial markers (CD31 and vWF) as detected by cytospin-immunostaining. Lewis lung carcinoma cells (LLC) were obtained from American Type Culture Collection (Manassas, VA, USA) and maintained in DMEM containing 10% FBS, 1% L-glutamine and antibiotics. All cell cultures were initiated from authenticated master frozen stocks, incubated at 37 °C in a humidified atmosphere containing 5% CO₂ and regularly tested for mycoplasma contamination. All reagents were purchased from Biochrom (Berlin, Germany).

4.2.2. EC proliferation and viability test

The synthesized derivatives were tested in vitro for their anti-

proliferative properties against EC by using the MTT assay that is based on the reduction of soluble MTT into blue-purple formazan crystals by metabolically active cells [46]. Briefly, EA.hy926 or HUVEC plated in 96-well plates at 4×10^3 cells/well in 100 μ L of complete medium were allowed to adhere for 24 h and then subjected to serum-starvation in medium containing 0.25% BSA (starvation medium) for 4 h. Subsequently, the cells were exposed to synthetic compounds or 0.1% v/v DMSO vehicle in presence of 2.5% FBS, 50 ng/mL of VEGF-165 or starvation medium alone for 24–48 h. At the end of treatment, MTT (Sigma, St. Louis, MO, USA) was added at 0.5 mg/mL and the cells further incubated for 4 h at 37 °C. The formazan crystals were solubilized by the addition of 0.1 N HCl in anhydrous isopropanol and the absorbance was measured on a microtiter plate reader at 595 nm with correction at 630 nm. The number of viable cells was determined by interpolation of OD values to respective standard cell growth curves.

Cell proliferation was also assessed under similar treatment conditions by using the CyQUANT[®] cell proliferation assay kit (Invitrogen, Waltham, MA, USA), according to manufacturer's instructions. Briefly, after treatment completion medium was removed from the wells, cells were carefully washed once with PBS, and then 200 μ L of CyQUANT GR dye/cell lysis buffer was added to each well and incubated for 5 min at room temperature, protected from light. The sample fluorescence was measured in a fluorescence microplate reader using excitation and emission filters at 480 and 520 nm, respectively and a reference standard curve was used for converting sample fluorescence to cell numbers.

Finally to check the potential cytotoxicity of test compounds under conditions applied for each of the following biological assays, cells were treated as specified and the number of viable cells was measured by the MTT assay.

4.2.3. IC₅₀ determination

IC₅₀ values for compound anti-proliferative activity were measured by the MTT assay as described above. Cells cultured in DMEM containing 2.5% FBS were exposed for 48 h to serial 1:2 dilutions of test compounds covering a concentration range of 0.125–50 μ M. IC₅₀ values (mean \pm SEM) were calculated from eight or more measured points using non-linear regression analysis.

4.2.4. Cell migration and Matrigel tube formation assays

HUVEC migration was evaluated using 8 μ m-pore size membrane Transwell chambers for 24-well plates (ThinCerts[™], Greiner Bio-One International GmbH, Kremsmuenster, Austria) as previously described [47]. Briefly, confluent cultures of serum-starved HUVEC grown in 6-well plates were pre-treated o/n with test compounds or vehicle solutions in medium containing 5% FBS. Cells were transferred to the upper chamber (6×10^4 cells/well) and left to migrate towards 5% FBS, VEGF-165 (50 ng/mL) or starvation medium added in the bottom chamber, for 6 h. Cells that have migrated to the lower side of the membrane were fixed with ice-cold ethanol, stained with haematoxylin for 5 min followed by eosin for 2 min, photographed and manually counted in five fields of view/well.

Formation of HUVEC tube-like structures was assessed by Matrigel assay as previously described [48]. Briefly, pre-starved HUVEC were seeded at 2×10^4 cell per well in 24-well plates pre-coated with 50 μ L of growth factor-reduced Matrigel (BD Biosciences, San Jose, CA, USA). Test compound or vehicle solutions were then added and cells further incubated for 24 h. Cells were fixed with ice-cold ethanol, stained with haematoxylin for 5 min followed by eosin for 2 min, photographed and the number of tube-like structures was scored in at least 5 fields of view/well.

Compound concentrations used in all these assays were previously shown to be non-cytotoxic.

4.2.5. Western blot

Serum-starved HUVEC cultured in 6-well plates were treated with 2 μ M of test compound or vehicle for 2 h followed by exposure to VEGF-165 (50 ng/mL) or PBS for 5 min. Cells were solubilized with lysis buffer (50 mM Tris-HCl, pH 7.6; 150 mM NaCl; 50 mM NaF; 0.5% sodium deoxycholate; 1 mM EDTA; 0.1 mM EGTA; 1% Triton-X; 0.1% sodium dodecyl sulfate (SDS); 1 mM phenylmethanesulfonyl fluoride; 1 mM Na₃VO₄; 0.1% protease inhibitor cocktail) and cell lysates containing equal amounts of protein were resolved by SDS-PAGE and immunoblotting as described before [49]. Primary antibodies used (Cell Signaling Technology, Danvers, MA, USA) specifically recognize the phosphorylated forms of VEGFR2 (Tyr 951, 996, 1056, 1175), AKT (Ser473), p38MAPK (Thr180/Tyr182) and ERK1/2 (Thr202/Tyr204, Thr185/Tyr187) or the total endogenous levels of the corresponding proteins. Immunoreactive bands were visualized by enhanced chemiluminescence detection (SuperSignal[™] West Pico Chemiluminescent Substrate kit, Thermo Scientific, Waltham, MA, USA). Gel-Pro Analyzer software (Media Cybernetics, Inc., Rockville, MD, USA) was used for densitometry.

4.2.6. LLC mouse tumor growth model

In vivo experiments were approved by the Veterinary Administration Bureau, Prefecture of Athens, Greece under compliance to the national law and the EU Directive 2010/63/EU for animal experiments. Male 6–8 week-old C57BL/6 mice (Hellenic Pasteur Institute, Athens, Greece) were assigned to separate groups of 5–6 mice and inoculated sc into the right flank with 5×10^5 viable LLC cells. Injections of test compounds at 0.05–0.2 mg/kg of body weight or vehicle were administered ip, thrice a week for 2 weeks, starting 24 h before implantation of tumor cells. Every other day tumor growth was monitored by electronic caliper measurement as described before [50] and mice were weighed and examined clinically for general condition. At end-point, animals were sacrificed, tumors and vital organs were excised and tissue samples were fixed in formalin.

4.2.7. IHC and histopathology

Slides of paraffin-embedded tissue sections were prepared and treated according to standard protocols. Next, sections were deparaffinized in xylene following rehydration in reducing degrees of absolute ethanol (100%, 96%, 70%) followed by washing in distilled water. For assessment of microvessel density, slides with tumor tissue sections were initially exposed to normal goat serum for 30 min at RT for blocking of non-specific binding sites and then incubated overnight at 4 °C with an anti-CD31 antibody (ab28364, Abcam, Cambridge, UK) at 1:100 [51]. Immunoreactivity was detected using the Vectastain ABC and DAB Peroxidase Substrate kit (Vector Laboratories, Burlingame, CA, USA) according to the manufacturer instructions. Immunoreactive cells were quantified in six different non-overlapping high-power fields. For estimation of compound toxicity, slides with tissue sections from vital organs (kidney, lung, spleen, liver, heart) were stained with haematoxylin-eosin and examined microscopically for histopathological alterations.

4.2.8. RNA isolation and qRT-PCR

Serum-starved confluent HUVEC grown in 6-well plates were treated with 2 μ M of test compound or vehicle in presence of 2.5% FBS for 6 h or 24 h. Total RNA was then isolated using the pureLink RNA Mini Kit (Ambion, Carlsbad, CA, USA) according to the manufacturer instructions. The quantification and quality analysis of RNA was performed on a Bioanalyzer 2100 (Agilent, Santa Clara, CA, USA).

For qRT-PCR, RNA (250 ng) was subjected to reverse

transcription using the Enhanced Avian First Strand synthesis kit (Sigma, St Louis, MO, USA) and qRT-PCR was performed using the KAPA SYBR Fast One-step qRT-PCR protocol (KapaBiosystems, Wilmington, MA, USA). Amplifications were performed in triplicate on a MJ RESEARCH PTC-200 qRT-PCR system, as follows: 95 °C for 5 min and 40 cycles of 95 °C for 5 s, 58 °C for 20 s and 72 °C for 5 s. The ribosomal protein RPS18S gene was used as the endogenous reference gene for all normalizations. Primers were provided by Eurofins Genomics (Ebersberg, Germany). The sequence of primers was as follows:

HMGCS1: Forward primer: 5'-CATTAGACCGCTGCTATTCTGTC-3' and Reverse primer: 5'-TTCAGCAACATCCGAGCTAGA-3',

MSMO1: Forward primer: 5'-ACATGGGAAAACCAATGGAA-3' and Reverse primer: 5'-TTCCAAATGGAGCCTGAAAC-3',

INSIG1: Forward primer: 5'-GCACTGCATTAACCTGTGG-3' and Reverse primer: 5'-GCAGCACTGAAATGAATGGA-3',

SQLE: Forward primer: 5'-TTAGAGGAGAAATGCCAAGGAA-3' and Reverse primer: 5'-CACTGATGAAGGAGGAAGGAAG-3',

UBE2C: Forward primer: 5'-TGATGCTGGCGATAAAGGGATT-3' and Reverse primer: 5'-GTGATAGCAGGCGTGAGGAA-3',

CCNB2: Forward primer: 5'-CCTCCCTTTTCAGTCCGC-3' and Reverse primer: 5'-CTCCTGTGTCATATTCTCCAAATC-3',

CCNA2: Forward primer: 5'-CTGCATTTGGCTGTGAACACTAC-3' and Reverse primer: 5'-ACAAACTCTGCTACTTCTGGG-3',

CDC20: Forward primer: 5'-GGCACCAGTGATCGACACATTCG-CAT-3' and Reverse primer: 5'-GCCATAGCCTCAGGGTCTCATCTGCT-3',

HMOX1: Forward primer: 5'-CTGCGTCTCTGCTCAACATC-3' and Reverse primer: 5'-GGGGCAGAATCTTGCACTTT-3',

RPS18S: Forward primer: 5'-TCGGAAGTGGCCATGA-3' and Reverse primer: 5'-GAACCTCCGACTTTTCGTTTC-3'

Ct values were automatically calculated by the machine's software and data analysis was performed by using the $2^{-\Delta\Delta CT}$ method [52].

4.2.9. Microarray hybridizations and functional analysis

Synthesis of cDNA and biotinylated cRNA was performed with the Illumina TotalPrep RNA Amplification Kit (Illumina, San Diego, CA, USA) using 500 ng of total RNA. Hybridization was performed onto Illumina Human-HT12 platform according to the manufacturer's instructions. The raw data were analyzed using packages lumi [53] and limma [54] in R computational environment. Briefly, method bgAdjust was used for correction, which estimates the background based on control probe information for between array correction, followed by variance adjustment based on bead level and mean-variance using variance stabilizing transformation (vst) for within array correction, and finally data normalization using the robust spline method (rsn), which combines the characteristics of quantile and loess algorithms. Significantly differentiated probe sets in compound-treated as compared to DMSO-treated cells were identified using a moderated paired *t*-test on linear models from limma, by applying the following thresholds: *p*-value < 0.05 and a fold change > |0.5| in log₂ scale. For functional analysis highlighting significant cellular processes based on GO, we used StRANER2 as described before [55].

4.2.10. Statistical analysis of cellular assays

The Mann-Whitney test was applied to determine the statistical significance of the data obtained and to compare the means between groups using GraphPad Prism 5.00 for Windows (GraphPad Software, San Diego, CA, USA). A *p* value of < 0.05 represented a statistically significant difference.

Conflict of interest disclosure

The authors declare no competing financial interest.

Authors declaration

All authors have participated significantly in the completion of the manuscript. OP, AC, FNK, PM, NP, HL: conceived and designed the experiments; MM, VG, VK, OP, GK, IKK, NL, HL: performed the experiments; MM, VG, VK, OP, GK, IKK, NL, AC, FNK, PM, NP, HL: analyzed the data; MM, PM, NP, HL: wrote the manuscript.

The final manuscript and authorship have been approved by all authors.

Acknowledgments

We thank Z. Kollia (Research Unit for animal standards, Evangelismos Hospital, Athens, Greece) for animal care assistance. We also gratefully acknowledge financial support from NSRF 2007–2013 National action, Cooperation sub-action II: SYNERGASIA 2009 PROGRAMME (09SYN-21-1078).

Appendix A. Supplementary data

Supplementary data related to this article can be found at <http://dx.doi.org/10.1016/j.ejmech.2016.05.035>.

References

- [1] J. Folkman, Angiogenesis: an organizing principle for drug discovery? *Nat. Rev. Drug Discov.* 6 (2007) 273–286.
- [2] L. Wang, G. Chen, X. Lu, S. Wang, S. Han, Y. Li, G. Ping, X. Jiang, H. Li, J. Yang, C. Wu, Novel chalcone derivatives as hypoxia-inducible factor (HIF)-1 inhibitor: synthesis, anti-invasive and anti-angiogenic properties, *Eur. J. Med. Chem.* 89 (2015) 88–97.
- [3] M. Romero, M. Zanuy, E. Rosell, M. Cascante, J. Piulats, M. Font-Bardia, J. Balzarini, E. De Clerq, M.D. Pujol, Optimization of xanthatin extraction from *Xanthium spinosum* L. and its cytotoxic, anti-angiogenesis and antiviral properties, *Eur. J. Med. Chem.* 90 (2015) 491–496.
- [4] D. Ravishankar, K.A. Watson, S.Y. Boateng, R.J. Green, F. Greco, H.M.I. Osborn, Exploring quercetin and luteolin derivatives as antiangiogenic agents, *Eur. J. Med. Chem.* 97 (2015) 259–274.
- [5] S. Salerno, A.M. Marini, G. Fornaciari, F. Simorini, C. La Motta, S. Taliani, S. Sartini, F. Da Settimo, A.N. García-Argáez, O. Gia, S. Cosconati, E. Novellino, P. D'Ocon, A. Fioravanti, P. Orlandi, G. Bocci, L. Dalla Via, Investigation of new 2-aryl substituted Benzo[thiopyrano][4,3-d]pyrimidines as kinase inhibitors targeting vascular endothelial growth factor receptor 2, *Eur. J. Med. Chem.* 103 (2015) 29–43.
- [6] Y. Shan, H. Gao, X. Shao, J. Wang, X. Pan, J. Zhang, Discovery of novel VEGFR-2 inhibitors. Part 5: exploration of diverse hinge-binding fragments via core-refining approach, *Eur. J. Med. Chem.* 103 (2015) 80–90.
- [7] N. Ferrara, H.-P. Gerber, J. LeCouter, The biology of VEGF and its receptors, *Nat. Med.* 9 (2003) 669–676.
- [8] C.K. Goldman, J. Kim, W.L. Wong, V. King, T. Brock, G.Y. Gillespie, Epidermal growth factor stimulates vascular endothelial growth factor production by human malignant glioma cells: a model of glioblastoma multiforme pathophysiology, *Mol. Biol. Cell* 4 (1993) 121–133.
- [9] H. Li, L. Fredriksson, X. Li, U. Eriksson, PDGF-D is a potent transforming and angiogenic growth factor, *Oncogene* 22 (2003) 1501–1510.
- [10] C. Lieu, J. Heymach, M. Overman, H. Tran, S. Kopetz, Beyond VEGF: inhibition of the fibroblast growth factor pathway and antiangiogenesis, *Clin. Cancer Res.* 17 (2011) 6130–6139.
- [11] A.-K. Olsson, A. Dimberg, J. Kreuger, L. Claesson-Welsh, VEGF receptor signalling in control of vascular function, *Nat. Rev. Mol. Cell Biol.* 7 (2006) 359–371.
- [12] M. Shibuya, L. Claesson-Welsh, Signal transduction by VEGF receptors in regulation of angiogenesis and lymphangiogenesis, *Exp. Cell Res.* 312 (2006) 549–560.
- [13] T. Takahashi, S. Yamaguchi, K. Chida, M. Shibuya, A single autophosphorylation site on KDR/Flk-1 is essential for VEGF-A-dependent activation of PLC- γ and DNA synthesis in vascular endothelial cells, *EMBO J.* 20 (2001) 2768–2778.
- [14] H. Zeng, S. Sanyal, D. Mukhopadhyay, Tyrosine residues 951 and 1059 of vascular endothelial growth factor receptor-2 (KDR) are essential for vascular permeability factor/vascular endothelial growth factor-induced endothelium migration and proliferation, respectively, *J. Biol. Chem.* 276 (2001)

- 32714–32719.
- [15] K. Holmqvist, M.J. Cross, C. Rolny, R. Hägerkvist, N. Rahimi, T. Matsumoto, L. Claesson-Welsh, M. Welsh, The adaptor protein Shb binds to tyrosine 1175 in vascular endothelial growth factor (VEGF) receptor-2 and regulates VEGF-dependent cellular migration, *J. Biol. Chem.* 279 (2004) 22267–22275.
- [16] T. Matsumoto, S. Bohman, J. Dixelius, T. Berge, A. Dimberg, P. Magnusson, L. Wang, C. Wikner, J.H. Qi, C. Wernstedt, J. Wu, S. Bruheim, H. Mugishima, D. Mukhopadhyay, A. Spurkland, L. Claesson-Welsh, VEGF receptor-2 Y951 signaling and a role for the adapter molecule TSAd in tumor angiogenesis, *EMBO J.* 24 (2005) 2342–2353.
- [17] N. Ferrara, K.J. Hillan, W. Novotny, Bevacizumab (Avastin), a humanized anti-VEGF monoclonal antibody for cancer therapy, *Biochem. Biophys. Res. Commun.* 333 (2005) 328–335.
- [18] Q.S.-C. Chu, Aflibercept (AVE0005): an alternative strategy for inhibiting tumour angiogenesis by vascular endothelial growth factors, *Expert Opin. Biol. Ther.* 9 (2009) 263–271.
- [19] F. Musumeci, M. Radi, C. Brullo, S. Schenone, Vascular endothelial growth factor (VEGF) receptors: drugs and new inhibitors, *J. Med. Chem.* 55 (2012) 10797–10822.
- [20] K.J. Gotink, H.M.W. Verheul, Anti-angiogenic tyrosine kinase inhibitors: what is their mechanism of action? *Angiogenesis* 13 (2010) 1–14.
- [21] G. Bergers, D. Hanahan, Modes of resistance to anti-angiogenic therapy, *Nat. Rev. Cancer* 8 (2008) 592–603.
- [22] M. Chauhan, R. Kumar, Medicinal attributes of pyrazolo[3,4-d]pyrimidines: a review, *Bioorg. Med. Chem.* 21 (2013) 5657–5668.
- [23] S. Schenone, M. Radi, F. Musumeci, C. Brullo, M. Botta, Biologically driven synthesis of pyrazolo[3,4-d]pyrimidines as protein kinase inhibitors: an old scaffold as a new tool for medicinal chemistry and chemical biology studies, *Chem. Rev.* 114 (2014) 7189–7238.
- [24] C. Peifer, S. Bühler, D. Hauser, K. Kinkel, F. Totzke, C. Schächtele, S. Laufer, Design, synthesis and characterization of N9/N7-substituted 6-aminopurines as VEGF-R and EGF-R inhibitors, *Eur. J. Med. Chem.* 44 (2009) 1788–1793.
- [25] S.B. Weitensteiner, J. Liebl, V. Krystof, L. Havlíček, T. Gucký, M. Strnad, R. Fürst, A.M. Vollmar, S. Zahler, Trisubstituted pyrazolopyrimidines as novel angiogenesis inhibitors, *PLoS One* 8 (2013) e54607.
- [26] Y. Dai, K. Hartandi, N.B. Soni, L.J. Pease, D.R. Reuter, A.M. Olson, D.J. Osterling, S.Z. Doktor, D.H. Albert, J.J. Bouska, K.B. Glaser, P.A. Marcotte, K.D. Stewart, S.K. Davidsen, M.R. Michaelides, Identification of aminopyrazolopyrimidine ureas as potent VEGFR/PDGFR multitargeted kinase inhibitors, *Bioorg. Med. Chem. Lett.* 18 (2008) 386–390.
- [27] Y. Oguro, N. Miyamoto, T. Takagi, K. Okada, Y. Awazu, H. Miki, A. Hori, K. Kamiyama, S. Imamura, N-Phenyl-N'-[4-(5H-pyrrolo[3,2-d]pyrimidin-4-yloxy)phenyl]ureas as novel inhibitors of VEGFR and FGFR kinases, *Bioorg. Med. Chem.* 18 (2010) 7150–7163.
- [28] Y. Oguro, N. Miyamoto, K. Okada, T. Takagi, H. Iwata, Y. Awazu, H. Miki, A. Hori, K. Kamiyama, S. Imamura, Design, synthesis, and evaluation of 5-methyl-4-phenoxy-5H-pyrrolo[3,2-d]pyrimidine derivatives: novel VEGFR2 kinase inhibitors binding to inactive kinase conformation, *Bioorg. Med. Chem.* 18 (2010) 7260–7273.
- [29] V.N. Kourafalos, P. Marakos, N. Pouli, L.B. Townsend, The synthesis of 4-deazaformycin A, *J. Org. Chem.* 68 (2003) 6466–6469.
- [30] S.S. Kadam, L. Maier, I. Kostakis, N. Pouli, J. Toušek, M. Nečas, P. Marakos, R. Marek, Synthesis and tautomerism of substituted pyrazolo[4,3-c]pyrazoles, *Eur. J. Org. Chem.* 2013 (2013) 6811–6822.
- [31] T. Tite, N. Lougiakis, P. Marakos, N. Pouli, The synthesis of 6-deazaformycin A, *Synlett* 18 (2009) 2027–2930.
- [32] L.N. Pino, W.S. Zehring, Preparation of pure 2-aminonitropyridines and 2-aminonitropicolines. Rapid separations by sublimation, *J. Am. Chem. Soc.* 77 (1955) 3154–3155.
- [33] A.G. Burton, P.J. Halls, A.R. Katritzky, The selective 3- and 5-nitration of 2-pyridones, *Tetrahedron Lett.* 12 (1971) 2211–2212.
- [34] A. Roe, R.B. Seligman, The preparation of 3-fluoroisonicotinic acid and related compounds, *J. Org. Chem.* 20 (1955) 1729–1732.
- [35] P. Marakos, N. Pouli, D.S. Wise, L.B. Townsend, A new and facile method for the preparation of 3-substituted pyrazolo[3,4-c]pyridines, *Synlett* 1997 (1997) 561–562.
- [36] D. Chapman, J. Hurst, Pyrazolopyridines. Part 5. Preparation and reactions of pyrazolo[3,4-c]pyridines, *J. Chem. Soc.* (1980) 2398–2404.
- [37] T. Ukai, H. Kawazura, Y. Ishii, J.J. Bonnet, J.A. Ibers, Chemistry of dibenzylideneacetone-palladium(0) complexes: I. Novel tris(dibenzylideneacetone)dipalladium(solvent) complexes and their reactions with quinones, *J. Organomet. Chem.* 65 (1974) 253–266.
- [38] X. Huang, K.W. Anderson, D. Zim, L. Jiang, A. Klapars, S.L. Buchwald, Expanding Pd-catalyzed C–N bond-forming processes: the first amidation of aryl sulfonates, aqueous amination, and complementarity with Cu-catalyzed reactions, *J. Am. Chem. Soc.* 125 (2003) 6653–6655.
- [39] E.J. Hanan, C. Eigenbrot, M.C. Bryan, D.J. Burdick, B.K. Chan, Y. Chen, J. Dotson, R.A. Heald, P.S. Jackson, H. La, M.D. Lainchbury, S. Malek, H.E. Purkey, G. Schaefer, S. Schmidt, E.M. Seward, S. Sideris, C. Tam, S. Wang, S.K. Yeap, I. Yen, J. Yin, C. Yu, I. Zilberleyb, T.P. Heffron, Discovery of selective and noncovalent diaminopyrimidine-based inhibitors of epidermal growth factor receptor containing the T790M resistance mutation, *J. Med. Chem.* 57 (2014) 10176–10191.
- [40] J. Xu, Y. Dang, Y.R. Ren, J.O. Liu, Cholesterol trafficking is required for mTOR activation in endothelial cells, *Proc. Natl. Acad. Sci. U. S. A.* 107 (2010) 4764–4769.
- [41] L. Fang, S.-H. Choi, J.S. Baek, C. Liu, F. Almazan, F. Ulrich, P. Wiesner, A. Taleb, E. Deer, J. Pattison, J. Torres-Vazquez, A.C. Li, Y.I. Miller, Control of angiogenesis by AIBP-mediated cholesterol efflux, *Nature* 498 (2013) 118–122.
- [42] F. Adah, H. Benghuzzi, M. Tucci, Cholesterol production inhibitor (statin) increased angiogenesis in surgically created femoral defect in an animal model, *Biomed. Sci. Instrum.* 50 (2014) 54–61.
- [43] G. Eelen, P. de Zeeuw, M. Simons, P. Carmeliet, Endothelial cell metabolism in normal and diseased vasculature, *Circ. Res.* 116 (2015) 1231–1244.
- [44] R.-H. Zhou, M. Yao, T.-S. Lee, Y. Zhu, M. Martins-Green, J.Y.-J. Shyy, Vascular endothelial growth factor activation of sterol regulatory element binding protein: a potential role in angiogenesis, *Circ. Res.* 95 (2004) 471–478.
- [45] M. Hatzia Apostolou, P. Katsoris, E. Papadimitriou, Different inhibitors of plasmin differentially affect angiostatin production and angiogenesis, *Eur. J. Pharmacol.* 460 (2003) 1–8.
- [46] T. Mosmann, Rapid colorimetric assay for cellular growth and survival: application to proliferation and cytotoxicity assays, *J. Immunol. Methods* 65 (1983) 55–63.
- [47] H. Loutrari, S. Magkouta, A. Papapetropoulos, C. Roussos, Mastic oil inhibits the metastatic phenotype of mouse lung adenocarcinoma cells, *Cancers* 3 (2011) 789–801.
- [48] M. Michailidou, H. Brown, D. Lefley, A. Evans, S. Cross, R. Coleman, N. Brown, I. Holen, Microvascular endothelial cell responses in vitro and in vivo: modulation by zoledronic acid and paclitaxel? *J. Vasc. Res.* 47 (2010) 481–493.
- [49] H. Loutrari, M. Hatzia Apostolou, V. Skouridou, E. Papadimitriou, C. Roussos, F.N. Kolisis, A. Papapetropoulos, Perillyl alcohol is an angiogenesis inhibitor, *J. Pharmacol. Exp. Ther.* 311 (2004) 568–575.
- [50] S. Magkouta, G. Stathopoulos, I. Psallidas, A. Papapetropoulos, F. Kolisis, C. Roussos, H. Loutrari, Protective effects of mastic oil from *Pistacia lentiscus* variation chia against experimental growth of lewis lung carcinoma, *Nutr. Cancer* 61 (2009) 640–648.
- [51] N. Weidner, J.P. Semple, W.R. Welch, J. Folkman, Tumor angiogenesis and metastasis - correlation in invasive breast carcinoma, *New Engl. J. Med.* 324 (1991) 1–8.
- [52] K.J. Livak, T.D. Schmittgen, Analysis of relative gene expression data using real-time quantitative PCR and the 2– $\Delta\Delta$ CT method, *Methods* 25 (2001) 402–408.
- [53] P. Du, W.A. Kibbe, S.M. Lin, lumi: a pipeline for processing Illumina microarray, *Bioinformatics* 24 (2008) 1547–1548.
- [54] M.E. Ritchie, B. Phipson, D. Wu, Y. Hu, C.W. Law, W. Shi, G.K. Smyth, Limma powers differential expression analyses for RNA-sequencing and microarray studies, *Nucleic Acids Res.* 43 (2015) e47–e47.
- [55] E.D. Pilalis, A.A. Chatziaoannou, Prioritized functional analysis of biological experiments using resampling and noise control methodologies, in: *Proceedings IEEE 13th International Conference on Bioinformatics and Bioengineering (BIBE)*, 2013, pp. 1–3.